Surface X-ray Diffraction Studies of Single Crystal Electrocatalysts

Yvonne Gründer and Christopher A. Lucas

Oliver Lodge Laboratory, Department of Physics, University of Liverpool,

Liverpool, L69 7ZE, UK

* Corresponding authors: yvonne.grunder@liv.ac.uk, clucas@liv.ac.uk

Abstract

In this article we review the contribution of surface x-ray diffraction (SXRD) to the topic of electrocatalysis. Based on several key examples it is shown how SXRD measurements elucidate the atomic structure at the polarised solid-liquid interface which can be used to develop a fundamental understanding of specific electrocatalytic reactions. The review begins with a discussion of single crystal gold electrodes and how the interplay of different adsorbates affects the lifting and formation of the reconstruction. This has given insight into the mechanism of the oxidation reactions on Au(*hkl*) surfaces. The second part of the review highlights the results obtained on Pt(*hkl*) single crystal surfaces, specifically the information obtained from SXRD measurements regarding the adsorption and oxidation of carbon monoxide. This includes the effects of anion adsorption, metal underpotential deposition and temperature changes. The third section gives a brief overview of bimetallic surfaces and how SXRD gives crucial information regarding both reactivity and the stability-reactivity relationship. The final section presents an outlook on current and future advances,

highlighting the possibility of accessing structural information about the liquid side of the interface and the aim of performing faster SXRD measurements to probe the time domain in electrochemical reactions. The development of experimental setups to study both reactive non-noble metal electrodes and surfaces with specifically engineered atomic geometries and composition for enhanced electrocatalytic reactivity is also described.

1. Introduction

In order to develop a fundamental understanding of electrocatalytic reactions and the corresponding structure-reactivity relationships, it is necessary to apply structural characterisation techniques that can determine atomic structure at the electrochemical interface *in-situ*, i.e. under reactive conditions. In this article we will focus on the use of surface x-ray diffraction (SXRD) measurements using synchrotron x-ray radiation to study the structure of extended single crystal surfaces in the electrochemical environment. The first synchrotron SXRD measurements of electrochemical systems were performed in the late 1980s and explored the phenomenon of underpotential deposition (UPD) [1, 2]. The methodology was further developed in the 1990s and, driven by improved procedures for the preparation and transfer of clean metal electrodes into the electrochemical x-ray cell, extended to studies of surface reconstruction (particularly of Au and Pt electrodes), anion adsorption and the influence of anion adsorption on the UPD process [3-10]. Comprehensive reviews of both the UPD and anion adsorption studies are given in reference [11] and reference [12] respectively. A more general review of the application of SXRD to electrochemical systems can be found in references [13, 14]. In this article we focus on the application of SXRD to electrocatalysis. Although SXRD is primarily a structure determination technique, correlation of the surface atomic structure to electrocatalytic reactions, driven by the applied electrode potential and/or the presence of reactive gases, is essential if a fundamental understanding of the reactions is to be obtained. Furthermore, SXRD can provide key information regarding structural changes during adsorption/desorption processes and may, in the future, enable the probing of electrocatalytic reactions in the time domain.

Table 1 lists some advantages and disadvantages of SXRD for application to the study of electrocatalysis. Perhaps the main disadvantage is that the technique is limited to the study

of well-ordered single crystal surfaces and cannot, at present, be applied to nanometer sized particles. Single crystals are, however, useful as model systems to explain the underlying atomic processes and elucidate specific (intermediate) well-defined adsorption sites. Another main disadvantage of the SXRD technique is the requirement of high intensity x-ray radiation, as the scattering from the buried solid-liquid interface is weak compared to that of a bulk crystal. Experiments therefore need to be performed at synchrotron facilities with appropriate experimental end stations and the time for one experiment is thus limited due to the competitive nature of gaining access to these facilities. These disadvantages, however, do not overshadow the main advantages of the SXRD technique in being able to obtain *in-situ* structural information on an atomic scale without having to disturb the system itself (although in certain situations the intense x-ray beam can have an effect on the measurements and this has to be considered on a case-to-case basis). Structural information of subsurface layers and the ionic arrangement in the electrolyte close to the interface can be achieved. In addition it is becoming possible to perform time resolved experiments to probe structural changes and obtain kinetic information. X-rays are used as the interaction probe with the interface and thus a combination of structural and spectroscopic x-ray techniques can also give insight into electronic structure. It should be noted that nanobeam synchrotron x-ray sources are currently under development and in the future it may become possible to probe individual nanoparticle surfaces; at present no such experiments have been performed.

In this article we present a selective review of SXRD experiments applied to electrocatalytic systems which incorporates both published work and some more recent results. The aim of the article is to illustrate the applicability of the SXRD technique to the study of electrocatalysis. Results selected from published papers are presented but for full details readers should refer to the cited work. After a brief review of the experimental methods (section 2), section 3.1 summarises experiments on single crystal Au electrodes in

alkaline electrolyte in which the potential-dependent forming and lifting of the Au surface reconstruction plays an important role. Section 3.2 presents an overview of the adsorption and oxidation of carbon monoxide on Pt(*hkl*) electrodes. Section 3.3 describes the application of SXRD to bimetallic surfaces where the issue of stability is key to the understanding of electrocatalytic reactivity [15, 16]. Finally in section 3.4 we describe some recent studies of more reactive electrodes with a look forward to potential future developments. This article concentrates on giving an overview of the importance to develop a structure-reactivity relationship by providing *in-situ* information about relaxation and reconstruction, the potential dependence of surface and adsorbate structure. For details about the electrocatalytic reactions that are discussed (mainly CO adsorption/oxidation and the oxygen reduction reaction) the reader is referred to articles in this special issue discussing those reactions [15, 17].

2. Experimental

It is beyond the scope of this article to provide a comprehensive description of SXRD and we refer the reader to reviews of the technique by Feidenhans'l [18], Fuoss and Brennan [19] and Robinson and Tweet [20]. Structural information, such as surface coverage, surface roughness and layer spacings (both adsorbate-substrate distances and the expansion/contraction of the substrate surface atoms themselves), of the electrode surface is obtained by measurement of the crystal truncation rods (CTR's). Through a combined analysis of the specular CTR results (where the momentum transfer, **Q,** is entirely along the surface normal direction) with non-specular CTR results (where **Q** has an additional in-plane contribution) a 3-dimensional picture of the atomic structure at the electrified interface can be obtained. Additional superstructure rods are observed for adlayers and for reconstructions of the first atomic layer(s) with a symmetry different from that of the underlying bulk crystal

lattice. In these cases the scattering from the surface or adlayer can be probed independently. Combining this independent structural information with CTR analysis a full picture of the interfacial structure, referenced to the underlying bulk substrate lattice, can be obtained [18, 20, 21]. The specular CTR probes the electron density distribution normal to the interface and does not require in-plane order, the measurement is therefore also sensitive to layering in the electrolyte side of the interface [22, 23]. No further explanation of the form of the CTRs is given in this review; non-specialist readers can find simple guides elsewhere [14, 24].

In this review we concentrate on SXRD studies of the three low index surfaces of metal crystals with the face centered cubic (*fcc*) crystal structure and the following indexing of the reciprocal space will be used throughout for the (111), (001) and (110) *fcc*-surfaces. The close-packed (111) surface has a hexagonal unit cell that is defined such that the surface normal is along the $(0, 0, l)_{hex}$ direction and the $(h, 0, 0)_{hex}$ and $(0, k, 0)_{hex}$ vectors lie in the plane of the surface and subtend 60°. The units for *h*, *k* and *l* are $a^*=b^*=4\pi/\sqrt{3}a_{NN}$ and $c^*=2\pi/\sqrt{6}a_{NN}$ where a_{NN} is the nearest-neighbor distance in the crystal. Due to the ABC stacking along the surface normal direction, the unit cell contains three monolayers and the Bragg reflections are spaced apart by multiples of three in *l*. The (001) surface is more open than the (111) surface and is indexed to a surface tetragonal unit cell. This is related to the conventional cubic unit cell by the transformations $(1, 0, 0)_t = 1/2(2, 2, 0)_c$, $(0, 1, 0)_t = 1/2(2, -2, 0)_c$ and $(0, 0, 1)_t = (0, 0, 1)_c$. The units for *h*, *k* and *l* are $a^*=b^*=2\pi/a_{NN}$ and $c^*=4\pi/\sqrt{2}a_{NN}$. Finally, the (110) reciprocal surface unit cell is rectangular and the reciprocal lattice notation is such that *h* is along [1 -1 0], *k* along [0 0 1] and *l* is along the [1 1 0] surface normal. The units for *h*, *k* and *l* are $a^*= c^*=2\pi/a_{NN}$ and $b^*=4\pi/\sqrt{2}a_{NN}$.

In addition to the analysis of CTR data, a particularly interesting application of SXRD is in potentiodynamic measurements, i.e. when the scattered x-ray intensity is measured at a particular reciprocal lattice position as the electrode potential is cycled over a given range.

We have termed this technique x-ray voltammetry (XRV) although a few alternative terms have been used in the literature. By measuring the XRV at a number of different CTR positions an insight into the nature of the structural changes, including dynamics and intermediate phases at the surface, can be obtained without having to perform a detailed measurement of the CTR profiles [25, 26]. The potential dependence of the scattered x-ray intensity from an ordered surface layer with a different symmetry to that of the underlying bulk crystal (e.g. surface reconstruction or adlayer) directly indicates the potential range of stability of the structure and potential dependent coverage. Subsequently features in the cyclic voltammetry (CV) can be directly correlated with structural changes at the electrode surface.

A key aspect in the study of single crystal metal electrodes is the preparation of the surface prior to the experiment and the transfer of the crystal into the electrochemical x-ray cell. Some specific crystals can be prepared by the flame-annealing technique [27-29]. A crystal with a flat, well oriented surface, is heated in a hydrogen or butane flame and then allowed to cool in air or hydrogen/argon before transfer to the electrochemical x-ray cell. This procedure has been successfully used for the preparation of Au and Pt surfaces. Other monometallic metal surfaces, such as Cu, Ag and Ni, cannot be prepared by flame-annealing methods. Alternatively the surface is prepared in a UHV environment by cycles of ion sputtering and annealing. This methodology has the advantage that the surface quality can be checked during preparation by standard surface science techniques, however the transfer into the *in-situ* x-ray cell has to be achieved without exposure to ambient atmosphere, especially for non-noble metals. UHV preparation is important for bimetallic surfaces for which precise surface compositions can depend on the annealing temperature. The most successful method for non-noble surfaces outside UHV has been with long pre-annealing in a forming gas, such

as hydrogen, followed by short electrochemical etching, rinsing with water and then direct transfer into the electrochemical x-ray cell [2, 30, 31].

3. Results and Discussion

3.1 Au(*hkl*) electrodes in alkaline electrolyte

Single crystal gold electrodes are model systems to demonstrate how SXRD has helped the understanding of electrochemistry and, more specifically, electrocatalysis. All three low-index Au(*hkl*) surfaces reconstruct at negative potential and the influence of pH and adsorbate species on the lifting and reforming of the reconstruction can be used to understand adsorbate-induced structural changes. This gives insight into the interaction between specific species in the electrolyte and the metal surface and its influence on electrocatalytic reactions. The lifting and formation of the reconstruction is accompanied by significant surface mass transport and a change in the surface symmetry giving rise to pronounced changes in the diffracted x-ray intensity.

Simplified real space models for the bulk-terminated and reconstructed low-index surfaces of gold are depicted in Figure 1. At negative potentials where the surfaces are (almost) free of strongly adsorbing anions the reconstructions of the Au(*hkl*) surfaces are observed. The reconstruction of the Au(111) surface involves a small increase in the surface density by compression of the first atomic layer along the <1 1 0> in-plane direction which leads to a large unit cell, with a (23 x √3) periodicity [7, 32]. The Au(001) surface also exhibits a hexagonal reconstruction of the first atomic layer. This layer is buckled and slightly distorted. The hexagonal structure is aligned close to the [110] bulk direction and is often referred to as a "5 x 20" or "hex" reconstruction [3, 33]. The Au(110) surface exhibits either (1 x 2) or (1 x 3) periodicity [7, 34]. For the (1 x 2) structure every other row is absent compared to the (1 x 1) phase and this reconstruction is referred to as the "missing row"

structure. The lifting of all three reconstructions is found to be potential-dependent and each surface has its own dynamics in the "reconstructed"↔ (1 x 1) conversion.

In this section we focus on SXRD studies of the reconstructions of the Au(111) and Au(001) surfaces. The corresponding surface-plane diffraction patterns for these two surfaces and the scattered intensity that arises due to the reconstruction in each case are shown schematically in Figure 2. Of particular interest is the behaviour of Au(001) in alkaline as well in acidic electrolytes. The potential range of stability and the dynamics of formation and lifting of the reconstructed phase in alkaline solution have been analyzed by a combination of SXRD and cyclic voltammetry [35]. A significant feature of the voltammetry in 0.1 M KOH, depicted in Figure 3(a), is the pseudocapacitance peak appearing at ~1.0 V. The sharp peak at 1.0 V was suggested to be associated with the potential/(OH_{ad})-induced lifting of the "hex" reconstruction, by analogy with the related peaks observed in acid solution containing strongly adsorbing anions [36]. Using density functional theory (DFT) calculations it was proposed that the lifting of the "hex" reconstruction is driven by adsorption rather than surface charge [37]. XRV measurements at the reconstruction-sensitive reciprocal space position, (1.2, 1.2, 0.1) - see Figure 2(b), further elucidated the structural potential behavior and possible adsorption processes. It was found that the onset of lifting of the "hex" phase takes place below 1.0 V (Figure 3(b)). The kinetics of "hex" formation are rather slow, as demonstrated in Figure 3(c) which shows the XRV measurement at the specular CTR position, sensitive to the mass transfer involved in the surface reconstruction.

Further insight into the "electric field *versus* adsorption" issue was obtained by studying the influence of co-adsorbates on OH-adsorption and reconstruction. The surface reconstruction was monitored under conditions in which strongly-adsorbed OH_{ad} is removed from the surface by a relatively weakly-adsorbed reactant, namely adsorbed carbon monoxide (denoted as CO_{ad}). Surprisingly it has been found that CO_{ad} acts to catalyze the formation of

uniform reconstructed domains. This phenomenon was established initially by STM studies of the Au(001) surface in alkaline solution [38] and was re-examined using SXRD. The key results are shown in Figure 3 which, in addition to the CV/XRV measurement in N_2-purged 0.1 M KOH solution, also summarizes the results in CO-saturated 0.1 M KOH. The SXRD results indicated that CO affects the kinetics of the formation and the potential region of stability of the reconstruction. The rather slow kinetics observed in N_2-purged alkaline solution are much faster in CO-saturated solution (Figure 3(c)) and the reconstruction is present over the entire potential range, i.e., up to 1.5 V. Gallagher *et al*. [39] showed that the CO-induced changes in the "reconstructed"↔(1 x 1) phase transition are a general phenomenon observed on all three Au single crystal surfaces. The extension of the potential region of stability is induced by continuous removal of strongly-adsorbed OH by weakly-adsorbed CO_{ad} in a Langmuir-Hinshelwood reaction, thus keeping the surface free of adsorbates over a more positive potential range. This confirms that lifting of the reconstruction is determined by adsorption rather than by the electric field.

Further evidence for this conclusion was obtained in acidic solution, where anions and OH_{ad} are in strong competition for the adsorption sites. Results were obtained for Au(001) in 0.1 M $HClO_4$ before and after Br^- anions were added to solution (Br^- anions are more strongly adsorbed than OH) [35]. The specific adsorption of Br^- shifts the equilibrium potential of the "hex" → (1 x 1) transition by ~0.3 V to less positive values, relative to Br^--free solution. SXRD data showed that the formation of uniform "hex" domains is not enhanced by this potential shift [40], although the specific adsorption of Br^- acts to catalyze the mobility of gold surface atoms. The "hex" → (1 x 1) transition is completed at ~0.1 V or, based on the x-ray intensity measured at (0.5, 1, 0.15), a position where an x-ray diffraction signal from the c($\sqrt{2}$ x 2$\sqrt{2}$)R45° Br_{ad} superstructure is observed, just prior to the formation of this structure. Thus it can be concluded that the "hex" → (1 x 1) transition is induced by the adsorption of

the bromide. The influence of CO on the phase transition in the presence of bromide was also investigated by SXRD and results obtained are plotted in Figure 4. CO has a negligible effect on the potential-dependent XRV measured at the (0, 0, 1.3) position in the presence of bromide (Figure 4(b)), i.e., in the presence of CO the "hex"↔(1 x 1) transition is shifted *negatively* by ~40 mV. In alkaline solution containing Br^-, however, a positive shift of the "hex"↔(1 x 1) transition induced by CO was observed [35]. This apparently opposite effect has been explained on the basis of a CO-induced increase in the equilibrium Br_{ad} surface coverage relative to that at the same potential in CO-free solution. As the same effect is also observed for the other two low-index Au single crystals it is possible to rationalize the effect of the pH on the "reconstructed"↔(1 x 1) transitions.

Blizanac *et al*. proposed that a delicate balance between the nature of the interaction of adsorbates with the Au(*hkl*) surface (the energetic part) and the potential-dependent surface coverage by anionic species controls the pH-dependent, CO effect [40]. The strength of the Au(*hkl*)-adsorbate interaction determines the energetic part: the Au(*hkl*)-CO interaction is much weaker than both the Au(*hkl*)-OH_{ad} interaction and the Au(*hkl*)-Br_{ad} interaction. Thus although CO cannot displace OH_{ad} and Br_{ad} from the Au(*hkl*) surface, in contrast to Br_{ad}, OH_{ad} can be oxidatively removed from the surface by CO in a Langmuir-Hinshelwood reaction. Consequently an increase in OH concentration (higher pH) stabilizes the potential range in which the surface reconstruction is observed, whereas Br, which is not consumed by CO, diminishes this potential range. The equilibrium surface coverage by Br_{ad} and thus the "equilibrium" potential for the "reconstructed"↔(1 x 1) transition is a consequence of the CO-correction to the adsorption isotherm of Br_{ad}. This is an important result in understanding the pH dependent and Br coverage kinetic effects on the oxygen reduction reaction (ORR) [41, 42]: whereas the energetic term of the Au-O_2^- interaction determines the potential region where the rate determining step of the addition of the first electron to the oxygen

accompanied by the adsorption of the oxygen occurs, the Bromide adsorption determines the availability of active sites for the adsorption of O_2^-.

Recently, the promoting effect of adsorbed carbon monoxide on the oxidation of alcohols by gold catalysts has been examined. Rodriguez, Koper and co-workers have described the enhanced catalytic properties in a series of papers [43-47]. It has been suggested that the presence of adsorbed CO can lead to OH adsorption at negative potentials in alkaline solution and this is the origin of the extraordinary electrocatalytic activity. The key effect is highlighted by the cyclic voltammetry (CV) measured after saturation of the surface with CO and subsequent purging of CO from the electrolyte. In this case, cycling the potential over a restricted range (so that the adsorbed CO is not oxidatively stripped from the Au surface) shows the appearance of a sharp reversible peak in the CV (not observed in the absence of pre-adsorbed CO) which has been attributed to the reversible adsorption of OH^- [43]. It is important to note that this voltammetric feature is only observed on hexagonal close-packed surfaces, i.e. the Au(111) surface and the reconstructed Au(001) surface [36, 39, 40, 48], and this suggests a fundamental link to the surface atomic structure.

The Au(111) surface has been carefully analysed by SXRD in the potential range of the reconstruction in the absence and presence of CO. Figure 5 shows the XRV measured at a sweep rate of 2mV/s, at the position where diffracted intensity from the reconstruction occurs, (0.019 1.019 0.3)-see Figure 2(a). A systematic change in intensity, which can be correlated with a structural change, between 0.4 V and 0.5 V (versus RHE) is clearly observed (note that this is not the lifting of the reconstruction which occurs at much higher potentials, ~1.1 V). This is at exactly the same potential where the reversible peak in the CV was observed after pre-adsorption of CO [43]. The transition is observed both on a CO-free and a CO-adsorbed surface (Figure 5(a) and 5(b) respectively). In both cases the relative change between 0.0 V and 0.7 V is ~15-20% of the maximum peak intensity. Given that it

has been shown that the scattering from the surface reconstruction arises from a single atomic Au layer [49], the decrease in intensity can only be attributed to an increase in the disorder, i.e. buckling of the reconstructed Au layer.

A detailed characterisation of the changes in the surface reconstruction can be obtained from the [H, K] scans shown in Figure 6, measured along the [1, 1, 0] direction through the (0, 1, 0.3) reciprocal lattice point (see Figure 2). Two clear peaks can be seen in each scan, a peak at H,K=0 corresponding to the scattering from the (0, 1, L) CTR and a peak at H,K~0.02 which arises due to the (p x √3) reconstruction. In these units the stripe separation in the reconstruction, p, is given by $p=1/(2\Delta H)$, where ΔH is the separation from the CTR position (at H=0), to the position of the reconstruction peak projected onto the H position [33] and this can vary as a function of the applied electrode potential [33]. Fits of a double Lorentzian lineshape to the data shown in Figure 6 enable the value of p to be obtained in each case. In the absence of CO, the values are found to be p=25.3±0.3 (0.25 V) and p=24.3±0.3 (0.7 V) whereas on the CO-adsorbed surface the values were found to be p= 22.8±0.4 (both at 0.25 V and 0.7 V), i.e. in the presence of CO there is no shift in the peak position. The structural changes indicated by the XRV data in Figure 5 can thus be summarised as follows: In the absence of CO the surface is reconstructed with a value of p~25 at 0.25 V and undergoes in-plane compression as a function of the applied potential reaching p~24 at 0.7 V. In the presence of CO no change in the surface compression is observed and the reconstruction is pinned into the (23 x √3) phase. Both with and without CO there is a decrease in the intensity of the reconstruction peak as the potential is increased. The intensity depends only on the density of the surface layer and the disordering (both thermal and static) which can be represented by a Debye-Waller factor [49]. The decrease in intensity is associated with an increase in the surface buckling of the Au layer resulting in an increase in static disorder. The reconstruction peak intensity measured in the presence of CO is also

lower than that observed in CO-free solution ***at any applied potential*** as this is the situation where the maximum compression (p~23) is observed.

In contrast to the results presented for Au(001), the SXRD measurements shown for the Au(111) surface were all obtained on the reconstructed surface. The high resolution of the SXRD technique means that very subtle changes in the surface structure can be followed as a function of the applied electrode potential. It is observed that adsorbed CO blocks the in-plane lateral movement of the surface Au atoms (observed in the absence of CO), i.e. the reconstruction maintains a (23 x √3) structure, identical to the structure that is observed under UHV conditions, over the entire potential range. Similarly to Au(001), adsorbed CO also acts to extend the potential range of stability of the Au(111) reconstruction [39]. Very recent measurements obtained in methanol electrolyte (0.1 M KOH + 2.5 M MeOH) have shown that the Au(111)-(23 x √3)-CO reconstruction is preserved during the oxidation of methanol (in contrast to the CO-free Au(111) reconstruction) and that the CO blocks the adsorption of the reaction intermediates/products [50]. The results for both Au(111) and Au(001) highlight the use of the SXRD measurements in understanding the subtle interplay between surface restructuring and adsorbate structures that determine electrocatalytic reactivity.

3.2 The adsorption and oxidation of carbon monoxide on Pt(*hkl*) electrodes

The catalytic properties of CO adsorbed onto platinum single crystals have been widely studied both in gas phase catalysis [51, 52] and electrocatalysis [13, 53]. This is because the system offers an opportunity to gain understanding that ultimately can lead to the design of new catalysts but also for understanding the activity of Pt metal nanoparticles in the size range of a few nanometers. Such nanoparticles are commonly employed as catalysts in a range of applications, particularly those related to low temperature hydrogen fuel cells [54,

55]. The interaction of carbon monoxide with Pt electrode surfaces is an important system for electrocatalysis as CO binds strongly to Pt and thus blocks active sites causing deterioration of the Pt catalyst. This is a big challenge for the use of Pt catalysts in fuel cell systems, further details can be found in this special issue [15]. SXRD measurements have been extremely important in the electrocatalysis studies of the CO/Pt system, as the adsorption and oxidation reactions can be monitored directly. Furthermore, the geometry of both the thin layer x-ray electrochemical cell, in which ~20 μm of electrolyte is trapped by a polypropylene film that is porous to gases, and the droplet x-ray electrochemical cell, in which the electrolyte droplet can be contained in any gaseous environment, means that measurements can be obtained with a constant supply of CO to the electrolyte so that the results are not compromised by the depletion of CO during the oxidation reaction.

In terms of the low-index Pt(*hkl*) electrode surfaces, SXRD studies have shown that the Pt(110) electrode surface can exhibit either the missing-row (1x2) reconstruction, as observed under UHV conditions, or an unreconstructed (1x1) termination, the exact structure that is formed depending on the cooling gas used during preparation by hydrogen flame annealing [56]. In contrast the 'hexagonal' reconstruction of the Pt(001) electrode surface, analogous to that observed on the Au(001) electrode surface, has not been observed in the electrochemical environment by any *in-situ* structural probes. The Pt(111) surface is unreconstructed at room temperature under UHV conditions and is also found to be unreconstructed in the electrochemical environment. In both acidic and alkaline electrolytes, the Pt(111)-(1x1), Pt(001)-(1x1), Pt(110)-(1x2) and Pt(110)-(1x1) surfaces are stable over the potential window defined by hydrogen evolution and oxide formation, the only potential-induced structural change being in the surface relaxation of the topmost Pt atomic layer [4, 6, 57]. Electrochemical studies have shown that on all Pt(*hkl*) electrode surfaces adsorption of carbon monoxide (CO_{ad}) leads to complete displacement of both underpotentially-deposited

hydrogen, H_{upd}, and any specifically adsorbed anions (e.g. HSO_4^-, OH^-). The driving force for the displacement of H_{upd} is the relative strength of the bonding, the Pt-CO_{ad} interaction being stronger than the Pt-H_{upd} interaction. On Pt(001), Pt(110)-(1x2) and Pt(110)-(1x2) surfaces the adsorption of CO_{ad} leads to significant changes in the surface relaxation of the topmost Pt atomic layer as observed by SXRD [56, 58]. This has enabled the CO adsorption and oxidation processes to be monitored indirectly through the changes in surface relaxation observed as a function of the applied potential. Although the results can be correlated with CV measurements, no direct information about the CO_{ad} layer could be obtained as no x-ray scattering features due to any ordered CO_{ad} were observed (as noted in the introduction, long-range order in an adsorbate structure is required for a detectable SXRD signal). This is probably due to the open nature and cubic (or rectangular) symmetry of the Pt(001) and Pt(110) surface structures. In contrast, on the close-packed Pt(111) surface, ordered hexagonal structures formed by the CO adlayer could be directly observed by SXRD measurements [25]. In this case SXRD is a powerful *in-situ* structural probe as illustrated in the selected results presented in this section.

The upper part of Figure 7 displays polarization curves for the oxidation of dissolved CO on Pt(111) in acid solution. According to Figure 7, two potential regions can be distinguished, a pre-ignition potential region followed by an ignition potential region. The term "ignition potential" is analogous to the term “ignition temperature” in gas-phase oxidation; it is the potential at which the rate becomes entirely mass transfer limited. Although the rate of CO oxidation changes with electrode potential, it has been suggested that in both the pre-ignition potential region, as well as at/above the ignition potential, the mechanism for CO oxidation obeys a Langmuir-Hinshelwood type reaction in which adsorbed CO reacts with adsorbed OH [59]. It was also proposed that the active sites for OH adsorption are defects in the Pt(111) surface [59].

The first *in-situ* determination of CO_{ad} structure was reported for a CO adlayer on Pt(111) in acidic electrolytes. Using *in-situ* STM, Villegas and Weaver [60, 61] observed a hexagonal close-packed (2 x 2)-3CO adlayer structure at potentials below 0.25 V (vs. SCE), with a CO coverage of Θ_{CO} = 0.75 ML. At potentials above 0 V (up to the onset of CO oxidation) a markedly different adlayer arrangement was formed, having a $\left(\sqrt{19}\times\sqrt{19}\right)R23.4^0-13CO$ unit cell with a CO coverage of θ_{CO} = 13/19 (hereafter abbreviated as the $\sqrt{19}$ structure). Following the STM studies, direct information regarding the CO_{ad} structure was obtained in SXRD measurements [62, 63]. Both the (2x2) and the $\sqrt{19}$ structures give rise to x-ray diffraction peaks that are separated from the scattering due to the Pt substrate and so the potential dependence of the structures and their ordering (i.e. domain size) can be measured directly [59, 64]. Figure 7(a) shows that the disappearance of the (2 x 2)-3CO structure at 0.7 V is accompanied by formation of the $\sqrt{19}$ structure which is stable even in the ignition potential region. This is a unique example where an adsorbate structure is present at a potential where maximum catalytic activity for an electrochemical reaction is observed. The SXRD results were used to explore the relationship between the surface coverage of spectator species and the rate of electrocatalytic reactions [65]. STM was used to identify the precise nature of the active sites for CO oxidation and a model for the electrocatalytic oxidation of CO was developed in which the active sites are in an array of nanopatches embedded in a closely packed (the $\sqrt{19}$ CO structure) spectator adlayer.

The structural models for both the (2 x 2) and $\sqrt{19}$ structures reveal that the (2 x 2) structure consists of three CO molecules per unit cell (θ_{CO} = 0.75) and the $\sqrt{19}$ structure contains 13 CO molecules, with a coverage, θ_{CO}, of 13/19 (θ_{CO} = 0.685). Based on the coverage-dependent heat of adsorption for CO on Pt(111), obtained from UHV data, it was postulated that the CO in the (2x2) structure is in a 'weakly-adsorbed' state and that the

reduction in CO coverage during the transition to the √19 structure leads to an increase in the Pt-CO interaction, i.e. CO_{ad} then being present in a strongly adsorbed state [63]. SXRD was used to derive a detailed structural model for the √19 structure and this is shown in Figure 8 [66]. The structural model of the Pt(111) surface relaxation induced by the $\sqrt{19}$ phase shows that different layer expansions and in-plane rotations occur for the Pt atoms under the near-top sites and the near bridge site CO molecules. The top view (Figure 8) shows how the 19 Pt atoms in the top-layer of the $\sqrt{19}$ unit cell are grouped into a motif that contains 7 Pt atoms in a centered-hexagon and 12 Pt atoms that are split between two triangular regions. Within each group, the Pt atoms are allowed to expand/contract laterally and to rotate around their center. For the underlying layers, the Pt atoms are assigned to either a centered-hexagon or a triangular region based on the ABC stacking sequence. This feature is illustrated schematically by the simplified "side view" shown in Figure 8. These results demonstrate that, if adsorption is relatively strong, then subsurface atoms can move collectively to form a pattern on the nanometer scale that is determined by the unit cell of an adlayer. The ability to probe the relaxation in sub-surface layers at the metal-electrolyte interface is unique to the SXRD technique and this kind of surface restructuring cannot be studied by any other experimental probe.

Considering that under practical conditions in fuel cells the electrooxidation of impure hydrogen (i.e. containing a trace of CO) may take place over the temperature range 273-363 K, an intriguing question to address is how the solution temperature affects the phase transitions in the CO structure. In order to introduce temperature control a new x-ray electrochemical cell was designed and the effects of temperature changes on the (2 x 2)↔ $\sqrt{19}$ phase transition in the CO adlayer on Pt(111) were examined [67]. As in the room temperature studies (Figure 7), the *temperature-controlled* (2 x 2) ↔ $\sqrt{19}$ phase transition was monitored by measuring the scattered x-ray intensities at (1/2, 1/2, 0.12) and (3/19,

14/19, 0.12) at 280 K, 293 K and 319 K and the results, together with the polarization curves, are summarized in Figure 9. Two significant new pieces of information arise from the measurements that give new insight into the interaction of CO with OH on the Pt(111) surface.

(1) The ordering of the (2 x 2)-3CO structure is frustrated under both "cold" (280 K) as well as "hot" (319 K) conditions. The fact that the integrated intensities and the widths (inversely related to coherent domain size) of the (2 x 2) peaks show a "volcano" relationship with the temperature of electrolyte may indicate that the balance between the rate of CO ordering and the surface coverage by OH (rate of CO oxidation) reaches a maximum at room temperature (293 K). Note also that the potential window of stability of the (2 x 2) structure decreases linearly by increasing the temperature, reflecting the negative shift in the onset of CO oxidation by increasing temperature (Figure 9(a)).

(2) The ordering of the $\sqrt{19}$ structure (i.e. coherent domain size) increases linearly by increasing the temperature, a consequence of enhanced OH adsorption at high temperatures [67]. At 319 K the $\sqrt{19}$ phase exists even at the onset of the hydrogen evolution reaction (at ~0 V). It is important to note that in the potential range where CO oxidation depends entirely on the rate of CO diffusion from bulk of the solution to the Pt surface, the $\sqrt{19}$ structure is rather stable. The rate of CO electrooxidation is a complex interplay between the desorption and readsorption of CO and oxygenated species, diffusion of coadsorbed CO and OH and the kinetics of the reaction between CO and oxygenated species [59]. The main effect of temperature appears to be on the kinetics of oxide formation, the activation of water and the adsorption of oxygenated species. These results open up new opportunities to establish correlations between temperature, structure, and surface reactivity that will be important for the future development of efficient energy conversion systems. For example, the stability of the metal catalysts used in low temperature hydrogen fuel cells is crucial to the longevity of

operation. Given that such devices operate at temperatures that are significantly higher than ambient, an understanding of the surface structure-reactivity relationships at elevated temperatures, for example in bimetallic systems, would be invaluable; it should be stated that this is not a trivial undertaking!

In determining the electrochemical reactivity of a surface towards a particular chemical reaction, it is clear that the electrode potential is key in determining the relative coverage by anion and/or cation species. For example, the coverage by anion species is an important factor in determining the rate of the ORR on transition metal surfaces [24]. An investigation into the effect of anions on the CO/Pt(111) system combined SXRD measurements with Fourier Transform Infrared Spectroscopy (FTIR) results [59]. This work illustrates the power of combining SXRD measurements with other *in-situ* techniques, such as FTIR (see, reference [68] in this issue for a detailed description of FTIR). It is important to note that the electrochemical interface is in chemical equilibrium and that adsorption/desorption processes are determined by the energies of adsorption unless kinetic barriers are present. This latter effect has been clearly illustrated in studies of the adsorption and oxidation of CO on Pt(*hkl*) surfaces modified by UPD metals. In these studies RRDE and SXRD measurements showed that UPD Cu and Pb are almost completely displaced from the Pt(001) and Pt(111) surfaces in perchloric acid (free of halide anions) by CO [25, 26]. Although these results are somewhat surprising and would not be observed in UHV studies, metal displacement can be understood from a simple thermodynamic analysis by calculating the Gibbs energy change (ΔG) for the component steps of the process [69]. These calculations predict the spontaneous displacement of Cu and Pb by CO from the Pt electrode due to the corresponding exothermicity of the overall ΔG. These results show that the nature of the metal-anion interaction and, hence, the strength of the adlayer-Pt bond, is crucial in determining the interaction with solution CO.

The goal of linking surface atomic structure to reactivity is shared both by electrochemists and the UHV heterogeneous catalysis community. The displacement results, however, highlight some clear differences between these two research areas that must be considered if common themes are to emerge. In particular, modification of an electrode surface by an UPD metal monolayer is not always equivalent to the UHV deposition counterpart, as the energetics of adatoms can be very different at the solid-liquid interface. This is clearly illustrated by the phenomenon of surface displacement which cannot be observed under non-equilibrium UHV conditions. An alternative to the creation of bimetallic surfaces by deposition of one metal onto another is to create a bulk bimetallic surface. In the following section we describe some examples of electrocatalysis on bimetallic surfaces.

3.3 Bimetallic surfaces

Bimetallic alloys systems are of great interest as electrocatalysts due to their enhanced reactivity, selectivity and resistance to poisoning compared to that of the parent metals. A knowledge of the surface structures formed by bulk bimetallic alloys has been gained by numerous studies using UHV techniques [70]. In electrocatalysis this has led to the study of well defined bimetallic surfaces, often prepared under UHV conditions and then transferred directly into the electrochemical environment [71]. In the electrochemical environment SXRD is the only technique that can give information regarding the surface and sub-surface atomic structure of the alloy material and this is essential to understand the electrocatalytic properties and develop a fundamental understanding of structure-function relationships. In this section we focus on two examples; $Pt_3Sn(111)$, which has been shown to be active for CO oxidation [72], and $Pt_3Ni(111)$, which has shown remarkable activity for the ORR [73]. In both cases, SXRD measurements have been crucial in characterizing the surface structure under reactive conditions and led to a fundamental understanding of the connections between

the atomic surface structure, the macroscopic kinetic rates of the reactions and the stability of the alloy surface in the electrochemical environment.

Pt_3Sn is an example of a bimetallic alloy which forms with an ordered sublattice of the constituent atoms with the *fcc* $AuCu_3$ structure. LEED studies of the $Pt_3Sn(111)$ surface prepared under UHV conditions indicated that the surface is truncated with the bulk structure, hence exhibiting a p(2x2) symmetry with respect to a pure Pt(111) surface plane with the surface composition matching the bulk (75% Pt, 25% Sn). SXRD was used to study the $Pt_3Sn(111)$ electrode after transfer from UHV into the x-ray electrochemical cell containing 0.5 M H_2SO_4 electrolyte [74, 75]. These measurements confirmed that the electrode surface structure remains intact during the transfer process and that the surface is stable over a potential range of ~1 V. Changes in the surface structure were then monitored as a function of potential and after saturation of the electrolyte with CO in order to study CO electrooxidation. In the presence of adsorbed hydrogen, H_{upd}, fits to the CTR data showed that the expansion of the surface Pt atoms induced by the adsorption of hydrogen was very similar to that observed on Pt(111), i.e. at 0.05 V, $\Delta d_{Pt}^{1,2} = \Delta d_{Sn}^{1,2} = +2\%$ [6, 62]. As shown in Figure 10, XRV results, measured at (1, 0, 3.6) and (1, 0, 4.3), indicate that the desorption of hydrogen, as well as the adsorption of bisulfate anions, leads to surface contraction, i.e. the interplanar spacing, shown as $d_{1,2}$ in the insert of Figure 10(b), decreases monotonically by scanning the potential positively from 0.05 V (measured versus RHE). At 0.55 V the Pt surface atoms are unrelaxed whereas the Sn atoms in the topmost layer expand, i.e. the surface becomes increasingly *buckled* as the Sn atoms expand outwards (at +0.55 V, $\Delta d_{Pt}^{1,2}$ =+0.5%, $\Delta d_{Sn}^{1,2}$ = +5.5%). Over the potential range shown in Figure 10, the changes in surface buckling are fully reversible. The buckling, however, is a precursor to Sn dissolution which occurs at potentials >0.55 V. This is indicated by a decrease in the measured x-ray signal at

(0, 1, 0.5), a CTR position sensitive to surface roughness [74]. This process is irreversible due to dissolution of Sn from the surface.

Similarly to the experiments on Pt(111) electrodes, described in section 3.2, CO adsorption/oxidation was also studied on the $Pt_3Sn(111)$ electrode. As for Pt(111) adsorption of CO in the H_{upd} region leads to complete displacement of the H_{upd} layer and replacement by CO_{ad}. In contrast to Pt(111), however, the adsorption of CO on the $Pt_3Sn(111)$ surface does not lead to the large surface relaxation (4%) observed on the Pt monometallic surface. This agrees with DFT calculations in which the binding energy of CO on $Pt_3Sn(111)$ was calculated to be weaker than on Pt(111) [76] and implies that CO is present in a 'weakly-adsorbed' state. X-ray voltammetry measurements in the presence of CO showed that the potential range of surface stability is extended compared to CO-free solution, an effect which strongly resembles the CO-controlled "reconstruction"$\leftrightarrow$(1 x 1) transition of Au(*hkl*) in alkaline solution (as discussed in section 3.1). In fact the onset potential for Sn dissolution increases from ~0.6 V (in CO-free electrolyte) to >1.0 V. It has been proposed that the reason for the increased potential range of stability of the $Pt_3Sn(111)$ surface in the presence of CO arises due to the continuous consumption of OH in the Langmuir-Hinshelwood reaction ($CO + OH_{ad} = CO_2 + H^+ + e^-$). In this reaction, OH is adsorbed onto Sn surface atoms whereas CO is exclusively adsorbed onto Pt surface atoms. The intermolecular repulsion between coadsorbed CO and OH species is the mechanism responsible for the high catalytic activity of $Pt_3Sn(111)$ for CO electrooxidation.

In contrast to the ordered alloy structure observed for Pt_3Sn, alloying of Pt with the 3d elements gives rise to crystal structures that are *fcc* but with a random occupation of lattice sites (in a ratio of occupancy that corresponds to the composition) by the constituent metals. The surface of these alloys can exhibit strong segregation effects which depend on the method of sample preparation. Bulk alloy materials were prepared by conventional

metallurgy and a systematic study of reactivity trends for polycrystalline Pt_3M (M=Ni, Co, Fe, Ti, V) surfaces was performed with the aim of developing new catalysts for the cathode side of the PEMFC [77]. The key results from these studies were; (i) the activity for the ORR, the cathodic half cell reaction in the polymer electrolyte membrane fuel cell, exhibited a 'volcano-type' dependence in relation to the measured surface electronic structure (the d-band center) and (ii) the segregated Pt-skin surface (100% Pt), produced by annealing, is 2-3 times more active than the corresponding sputtered surfaces (with bulk alloy surface composition). This systematic study confirmed earlier work on PtM polycrystalline alloys which had indicated that Pt-skin layer formation enhances the activity for the ORR [78] and that the enhancement is linked to changes in the Pt-skin electronic structure [79, 80]. In an extension of this work to single crystal surfaces, it was found that the $Pt_3Ni(111)$ surface has the highest activity that has ever been observed on a cathode catalyst, with a specific activity 10-fold higher than Pt(111) and 90-fold higher than the current state-of-the-art Pt/C catalysts [73]. In order to understand such remarkable activity it is important to know the surface atomic structure and stability in the reactive environment and this is where SXRD measurements have provided crucial structural information [81].

The $Pt_3Ni(111)$ surface was prepared in UHV by cycles of sputtering and annealing, a final anneal resulting in a Pt-rich surface as confirmed by low energy ion scattering. The sample was then transferred into the x-ray electrochemical cell and contacted at 0.05 V in 0.1 M $HClO_4$ electrolyte. Figure 11(a) shows the (0, 0, *l*) and (0, 1, *l*) CTR data measured at 0.05 V and the best fit to the data obtained by an atomic model. The model assumes the crystal to be a perfectly random alloy with an *fcc* lattice, each atom having an average atomic form factor of $0.75\ f_{Pt} + 0.25\ f_{Ni}$ [82]. In order to provide uniqueness in the modeling of the CTR data, energy dependent measurements at two reciprocal lattice positions were performed. The data points in Figure 11(b) correspond to integrated intensities at (0, 0, 3.3) and (0, 0, 1.5) as

a function of the incident x-ray energy. From this data an intensity ratio at each CTR position, I_{8323eV}/I_{8133eV}, was calculated and the results are plotted in the inset to Figure 11(a). By simultaneously fitting this ratio data which constrains the fit to the full CTR data, sensitivity to the elemental concentration profile at the surface, i.e. separation from surface roughness effects in the modeling of the CTR data, is obtained.

The dashed line (black) is a calculation of a perfectly terminated $Pt_3Ni(111)$ crystal with a Pt-skin. The best fit to both CTR data and the ratio data is shown by the solid green line in Figure 11(a). The surface atomic layer is thus determined to be 100% Pt, the second atomic layer to be 48% Pt, the third to be 87% and beyond that the bulk value of 75%. It is clear from these results that the Pt-rich segregated surface (as determined using low energy ion scattering during preparation in the UHV chamber) is stable both during transfer from UHV and, subsequently, in the electrochemical environment. Furthermore, the CTR measurements also prove the composition of the sub-surface atomic layers and indicate that the second atomic layer is Ni-rich compared to the bulk alloy composition. This is key in understanding the modified electronic properties of the surface Pt layer (compared to bulk Pt(111)) which determines the surface reactivity.

Following the determination of the surface atomic structure, the potential dependence of the surface was investigated using x-ray voltammetry (XRV) and cyclic voltammetry (CV). Results were obtained for both the $Pt_3Ni(111)$ sample and a Pt(111) electrode for comparison and representative results are shown in Figure 12. The potential response of the two surfaces (Figure 12(b)) can be separated into three regions; the first corresponds to the underpotential deposition of atomic hydrogen on the surface (H_{upd}), the intermediate region to the charging of the double layer and the positive potential region to the reversible adsorption of OH (OH_{ad}). Integration of the charge in the CV gives the surface coverages by H_{upd} and OH_{ad} and these are shown in Figure 12(b). There is a negative potential shift of ~0.15 V in

H_{upd} and a positive potential shift of ~0.1 V in OH_{ad} on the Pt-skin surface relative to the Pt(111) surface. Figure 12(a) shows the XRV's for the $Pt_3Ni(111)$ surface measured at (0, 0, 2.7) and for the Pt(111) surface at (1, 0, 3.6). Both of these reciprocal lattice positions, at *l* values just below a bulk Bragg reflection, are sensitive to surface relaxation as confirmed by the corresponding measurements at *l* values above the Bragg reflections, (0, 0, 3.3) and (1, 0, 4.4), which showed 'mirror-like' behavior. For this reason the intensities are converted to surface expansion (by model calculations after fits to the full CTR data sets in each case) normalized to the values obtained at 0.05 V. It is important to note that at 0.05 V the Pt(111) surface is expanded by ~2% of the lattice spacing whereas the $Pt_3Ni(111)$ surface is essentially unrelaxed. Figure 12(a) shows the change in expansion relative to the value measured at 0.0 V, i.e. the pure Pt(111) surface is expanded by ~2% at 0.0 V and this is reduced to ~1.5% expansion at 0.8 V, whereas the $Pt_3Ni(111)$ surface is unrelaxed at 0.0 V and undergoes a ~1.5% contraction at 1.0 V.

Surface expansion is dependent on the substrate-adsorbate bondstrength, i.e. the chemisorption properties that depend on the surface electronic structure (the d-band center) [83]. On both Pt(111) and $Pt_3Ni(111)$ the adsorption of OH_{ad} causes surface contraction (the shift in the potential for OH_{ad} is clearly seen in Figure 12) and this is the precursor to oxide formation via place exchange with the Pt surface atoms [84]. The hysteresis observed for Pt(111) is large and is presumably due to the fact that the relaxation not only depends on the coverage but also the ordering of the adlayer species. The structural changes are thus dependent on the kinetics of ordering on the surface, a process that can have a timescale of several minutes [85]. The reduced hysteresis on the $Pt_3Ni(111)$ surface is likely due to the weaker metal-adsorbate interaction. The stability of the $Pt_3Ni(111)$ surface is a consequence of the electronic structure (d-band center) that decreases the amount of OH_{ad} (Figure 12(b)) so that there is less tendency for place exchange and irreversible roughening. This mechanism

is also responsible for the increased activity for the ORR. The close packed nature of the (111) surface helps to prevent the dissolution of Ni from the sub-surface layer and preserve the activity for the ORR.

3.4 Recent developments and outlook

So far in this article we have focused on the surface structures observed on Au, Pt and Pt-based alloy single crystal electrodes. A key quality that has emerged from these studies is that the surfaces are stable, provided that the applied potential is restricted to a certain range away from irreversible reactions such as oxide formation [91]. Experimentally, this is advantageous in that detailed SXRD measurements from a particular system can be obtained in a timescale over which the surface undergoes no irreversible structural modification. More reactive metal surfaces present a greater challenge due to the problems associated with the transfer of a prepared crystal into the x-ray electrochemical cell and the stability of the surface in the electrochemical environment. One way to overcome the transfer problem is to use a portable chamber which can be connected to a docking port of a main UHV chamber. One example is the TRECXI chamber [86] which has portable UHV ion pumps to maintain the UHV conditions and a large cylindrical Be window to allow the incident and scattered x-ray beams to pass through the chamber. An electrochemical cell can then be mounted above a UHV valve on top of the Be cylinder and can be lowered toward the sample once the chamber is filled with inert gas at ambient temperature and the UHV valve is open. The electrochemical cell in this setup consists of a glass tube (about 25 cm long) that has an open end for forming a droplet of electrolyte on one side and is connected to a glass cross on the other side. The glass cross contains connectors for the electrochemical inlet and outlet tubings, the counter-electrode (Pt wire) and a reference electrode (a commercial Ag/AgCl microelectrode). Such equipment has been used for SXRD studies of a number of UHV-

prepared electrode surfaces, for example, for studying both the adsorption of water onto Pt(111) and the electrochemistry of a $Pt_3Sn(111)$ surface alloy [87, 88] and for studies of the dissolution of a Cu_3Au alloy crystal [89]. There is scope for many future experiments which involve transfer of a surface prepared under UHV conditions to the electrochemical environment. UHV preparation can allow precise control of surface stoichometry in materials such as complex intermetallic alloys or perovskites. We note that perovskite materials show great promise for application in electrocatalysis [90, 91] and yet the development of detailed surface structure-function relationships, vital to designing real catalyst materials for applications, remains a distant goal. Furthermore it may be possible to embed catalytically active elements into a relatively inert surrounding, thereby overcoming the intrinsic detrimental link between surface reactivity and surface stability. In the future this may enable controlled studies of the metal-support interaction [92] in the electrochemical environment.

As noted throughout this article, whereas SXRD requires structures to possess long-range order in order for the diffraction signal to be measureable, the specular CTR (sometimes called extended x-ray reflectivity) has no such limitations and can be very sensitive to ordering in the electrolyte side of the interface, i.e. layering that occurs at the solid-liquid interface [23, 93]. The first such study of layering at the electrochemical interface was reported by Toney *et al*. [93, 94], where it was proposed that a dense ice-like water layer was present in non-adsorbing electrolyte (0.1 M NaF) on a Ag(111) electrode. In relation to electrocatalysis such measurements have recently become of renewed interest after it was shown that hydrated cation species can form a non-covalent bond with adsorbed anions, such as OH^-, and thus influence the rate of electrocatalytic reactions by their presence in the electrochemical double layer [95]. Measurements of a Ag(111) electrode in alkaline electrolyte confirmed this hypothesis as illustrated by the results shown in Figure 13 [22]. Whereas the non-specular CTR data (Figure 13(b)(d)) shows only a small potential dependent

change, which can be modeled by a change in relaxation at the Ag(111) surface, the specular CTR data shows a large potential-dependent change which is due to strong ordering effects in the electrochemical double layer. The data are consistent with the structural model shown in Figure 13, i.e. at negative potential (-1.0 V) there is no chemisorbed species and a hydrated cation layer is present at a distance of 4.1 Å above the Ag surface, whereas at -0.2 V adsorbed hydroxide stabilizes the cation layer at a distance of 3.6 Å through a non-covalent (van der Waal's) interaction. Similar measurements were also made on a Ag(001) electrode where it was shown that adsorbed bromide anions induce the coadsorption of hydrated Cs^+ cations with the Br_{ad}-Cs^+ interlayer spacing being dependent on the electrode potential due to repulsive electrostatic forces [96]. Resonant x-ray scattering measurements made on the specular CTR were used to illustrate the presence of a partially hydrated Ba^{2+} cation layer at the Pt(111) electrode surface in alkaline solution (0.1 M KOH) [97]. In this study the resonant x-ray technique enabled the presence and location of the Ba^{2+} cations to be determined even in the presence of K^+ cations. Furthermore the measurements were used to demonstrate that the hydrated cations have a significant effect on the ORR on Pt surfaces whereas the effect on Au surfaces is relatively small. This may be linked to the fact that only the Au(*hkl*) surfaces and not the Pt(*hkl*) surfaces exhibit potential-dependent surface reconstruction in the electrochemical environment. In future studies it would be interesting to probe the electrolyte ordering under ORR conditions. Such measurements may give additional insight into the nature of the oxygenated species at the interface (as described for Pt(111) in this special issue [98]).

Being able to get structural information about the ion ordering in the double layer and, more specifically, the interaction and solvation energies associated with this ordering may lead to a better understanding of electrocatalytic reactions in non-aqueous electrochemistry. This could be greatly helped by combination with spectroscopic tools (for example as shown

by the resonant x-ray results) to not only get structural information but also chemical information about the ions and their oxidation states. The application of SXRD techniques to study non-aqueous electrochemistry may enable a fundamental understanding of systems relevant to future battery technologies for example. We also note that extended x-ray reflectivity measurements in ionic liquids (ILs) have shown strong liquid layering effects at a charged solid electrode surface [99]. The study of ordering phenomena in ILs could be a rich area for future studies with a range of electrochemical applications.

Finally it is apparent that the improved brilliance of the synchrotron sources over the last decade has led to the possibility of probing the time domain in electrochemical systems [100-103]. So far time-resolved studies have been limited to electrodeposition and electrodissolution systems, as changes in the metal side of the interface can cause large changes in the diffracted x-ray intensity. For example, in a study of the electrochemical dissolution of Au(001), data was obtained at an acquisition rate of ~100 Hz enabling real time measurements of Au dissolution up to rates of ~20 monolayers/second [101]. Given that many electrocatalytic reactions are fully reversible it may become possible to explore the time domain by using lock-in amplifier techniques, whereby the measured x-ray signal is phase matched to the applied electrode potential. Thus accessing molecular scale processes at the electrochemical interface, including the ordering and dynamics of the electrolyte by a combination of spectroscopic and structural x-ray techniques at shorter timescales may soon become possible. One could even envisage experiments which utilize the fourth generation of light sources, x-ray free electron lasers (XFELS)-truly an exciting prospect!

4. Conclusions

Over the last couple of decades in-situ SXRD has played a key role in the development of structure-reactivity relationships in electrocatalysis. This has principally been

due to the ability to determine the atomic structure at electrode surfaces in the electrochemical environment in which the electrocatalytic reactions occur. In this short review we have presented some key results that highlight the role of the SXRD measurements in establishing a fundamental understanding of electrocatalysis. The nature of the SXRD technique is that it requires the use of single crystal electrodes and thus the structural data can be correlated with adsorption of species onto well defined surface sites. Particular information that the SXRD measurements have provided includes (i) surface reconstruction and relaxation phenomena, (ii) understanding the potential dependence of surface structures, (iii) correlations that have been established between surface structure and the energetics of adsorption, (iv) the structures formed by adsorbates and their influence on electrochemical reactivity, (v) the fact that CO adsorption can lead to some surprising effects in electrochemistry, such as the enhancement of surface reconstruction and the displacement of adsorbed metal layers, (vi) the relationship between stability and reactivity and (vii) the influence of the both the inner and outer Helmholtz planes that form the electrochemical double layer structure on electrocatalytic reactions.

Nowadays there are many synchrotron sources around the world that are providing intense and stable x-ray beams. Also methods of sample preparation have greatly improved since the first SXRD experiments performed at synchrotron sources in the late 1980s. As a result, measurements that were once challenging are now relatively routine. We hope that this review will act as a stimulus for further studies. As the emphasis of surface science studies using synchrotron radiation continues to shift away from the UHV-characterization of surface structures to explore the relationship between structure and functionality, the electrochemical interface will continue to be at the forefront of such research.

Acknowledgements

We would like to thank Nenad Markovic (Argonne National Laboratory) for many years of fruitful collaboration and for inspiration in this field of research. CAL acknowledges all co-workers (too many to list by name) in Nenad's groups who were involved in the work both at Lawrence Berkeley National Laboratory and, more recently, Argonne National Laboratory. Similarly YG would like to acknowledge her co-workers at CAU, Kiel within the group of Olaf Magnussen. We would like to thank the XMaS beamline staff for their support of the XMaS beamline at the ESRF. The XMaS beamline is an EPSRC mid-range facility managed by the University of Liverpool and the University of Warwick. We would also like to thank all of the scientists that we have interacted with and the support staff at the synchrotrons that we have used over the last few years, namely SSRL, APS, ESRF and the Diamond Light Source. Finally we thank a number of PhD students at the University of Liverpool for their contribution to this work. In chronological order they are Matthew Ball, Mark Gallagher, Ben Fowler, Mick Cormack, Alex Brownrigg, Michael Darlington, Naomi Sisson, Gary Harlow and Liz Cocklin. YG and CAL acknowledge the financial support of the EPSRC (UK). YG acknowledges the financial support of the Royal Society (UK) through a University Research Fellowship.

Advantages	***Disadvantages***
3D characterization of interface structure (including the liquid side)	High intensity x-ray beam required (i.e. needs a synchrotron x-ray source)
In-situ, non-destructive technique	Influence of the intense x-ray beam on the structure/electrochemistry?
Possible chemical information through x-ray spectroscopic methods	Limited to single crystal surfaces
Combination with other *in-situ* methods is possible	Specific experimental setup (including diffractometer) required
Relatively easy to control environment (e.g. gases, temperature, flow cells, etc)	Requires a stable system for detailed characterization
Time resolution is possible	Limited access time to synchrotron source

Table 1. Advantages and disadvantages of the surface x-ray diffraction technique for the study of electrocatalysis.

Figure Captions

Figure 1. Simplified real space model of reconstructed (right side) and bulk terminated (left side) Au(*hkl*) surfaces: Au(001)-(5 x 20) $\leftrightarrow$ (1 x 1); Au(111)- (23x$\sqrt{3}$) $\leftrightarrow$ (1 x 1) ; Au(110)(1 x 2) $\leftrightarrow$ (1 x 1).

Figure 2. Reciprocal space maps of the surface plane scattering observed for **(a)** the Au(111) and **(b)** the Au(001) surfaces, indicating where scattering from the reconstructed surfaces arises.

Figure 3. (a) The cyclic voltammetry for Au(001) in 0.1 M KOH along with the polarization curve for CO oxidation in CO-saturated solution (grey curve); **(b)** XRV measured at the reconstruction position, (1.206, 1.206, 0.4), in CO-free (dashed curve) and CO-saturated (solid line) solution; **(c)** XRV measured at a position sensitive to the mass transfer involved in the surface reconstruction, (0, 0, 1.3), with and without CO in solution (reproduced with permission from reference [39]).

Figure 4. (a) Current-potential curves (first scan) for Au(001) in 0.1 M $HClO_4$ + 10^{-3} M Br^- purged either with argon (blue curve) or CO (red curve) at 10 mV/s. **(b)** Corresponding XRV measurements (2 mV/s) at (0, 0, 1.3), a position on the specular CTR; **(c)** XRV measurements (2 mV/s) at (0.5, 1, 0.15), where scattering from the c($\sqrt{2}$ x 2$\sqrt{2}$)R45° structure of Br_{ad} is observed (reproduced with permission from reference [35]).

Figure 5. X-ray voltammetry monitoring changes in the gold surface reconstruction measured at (0.019, 1.019, 0.3) **(a)** in 0.1 M KOH free of CO and **(b)** after CO adsorption at

0.25 V and purging of the electrolyte with N_2. The x-ray signal has been background subtracted, i.e. the lifting of the reconstruction would cause the intensity to drop to zero on this scale. The sweep rate for these measurements was 2 mV/sec.

Figure 6. In plane x-ray diffraction from the reconstructed Au(111) surface measured along the [1, 1, 0] direction at 0.7 V and 0.25 V (vs RHE). The data is fitted with a double Lorentzian line profile (see text for details). **(a)** in 0.1 M KOH free of CO and **(b)** after CO adsorption at 0.25 V and purging of the electrolyte with N_2. The data and fits at 0.7 V are shown in blue and those at 0.25 V are shown in red. The dashed vertical line indicates the peak position measured at 0.25 V in CO-free solution.

Figure 7. (Top) The polarization curve for CO oxidation for Pt(111) in CO-saturated 0.1 M $HClO_4$ solution at 298 K (sweep rate 2 mV/s). **(Inset)** A close-up of the pre-oxidation potential region showing the first and second anodic sweeps. **(Bottom)** X-ray Voltammetry measured at the (½,½, 0.12) and (3/19, 14/19, 0.12) positions where x-ray scattering arises due to the (2 x 2)-3CO and (√19 x √19)-13CO structures respectively. Schematics of the CO structures, indicating the unit cells, are shown in between the two panels (adapted with permission from reference [13]).

Figure 8. Structural model of the Pt(111) surface relaxation induced by the (√19 x √19)-13CO phase. Small solid and open circles represent the CO molecules in nearly top and bridge sites, respectively. Large circles in different colors represent the Pt atoms in three groups with different rotation centers. The "side view" is not a projection, but a simplified picture to illustrate schematically the grouping and layer expansion. The top layer expansions

of 0.28 and 0.04 from the lattice positions are amplified 4-fold for simplicity (reproduced with permission from reference [66]).

Figure 9. Temperature effects on the structure and oxidation of carbon monoxide on the Pt(111) electrode in 0.1M $HClO_4$. **(a)** Polarization curves indicating the temperature-controlled CO oxidation reaction in the pre-ignition potential region and at the ignition potential. Note that at 279 K (green data) the diffusion limiting current for CO oxidation is not reached. **(a')** Enlargement of the pre-ignition region showing enhanced CO oxidation at higher temperatures. **(b)** XRV measured at a CO-(2x2) peak (only anodic sweeps are shown) as a function of temperature. **(b')** the integrated intensity (arb. units) and domain size (nm) of the CO-(2x2) structure measured at 0.05 V as a function of temperature. **(c)** XRV measured at a CO-√19 peak (only anodic sweeps are shown) as a function of temperature. **(c')** the integrated intensity (arb. units) and domain size (nm) of the CO-√19 structure measured at 0.9 V as a function of temperature. Note that at 319 K the (2x2) and √19 structures are coexistent at 0.05 V whereas at 279 K the structures are coexistent at 0.9 V. Red data corresponds to data measured at 319 K, green data at 293 K (room temperature) and blue data at 279 K. All of the results were obtained after several cycles of the electrode potential over the full potential range shown. (reproduced with permission from reference [67]).

Figure 10. (a) Cyclic voltammograms of Pt(111) (dashed gray line) and Pt_3Sn(111) (solid red line) in 0.5 M H_2SO_4, scan rate 50 mV/s. Potential-dependent integrated charges for the adsorption of (bi)sulfate anions on the Pt_3Sn(111) surface are represented by circles. **(b)** The measured x-ray intensities at (1, 0, 3.7) and (1, 0, 4.3) as a function of the electrode potential. Top and side views represent the proposed p(2 x 2) structure. The gray circles are Pt atoms, the black circles are Sn atoms and triangles are (bi)sulfate anions which are adsorbed on Pt

sites. The side view indicates the surface normal spacing that is derived from CTR measurements (reproduced with permission from reference [75]).

Figure 11. Crystal Truncation Rod (CTR) data of the $Pt_3Ni(111)$ crystal surface in 0.1M $HClO_4$ with an applied potential of 0.05 V (vs. RHE). **a)** The circles are the data points and the solid line (green) is the best fit to the data. The dotted line (black) is a calculation of a perfectly terminated $Pt_3Ni(111)$ crystal with a Pt-skin, and the dot-dot-dash line (red) is a calculation of a $Pt_3Ni(111)$ crystal with a Pt-skin and including the fit parameters. Inset) Energy ratio data as described in the text. Again the data points are denoted by circles and the best fit to the data is a sold line (green). The dotted (blue) line is a calculation of a perfectly terminated $Pt_3Ni(111)$ crystal and the dashed (black) line is a calculation of $Pt_3Ni(111)$ crystal with a Pt-skin. **b)** Measurements at the (0, 0, 1.5) and (0, 0, 3.3) reciprocal lattice positions as a function of the incident x-ray energy. The vertical dashed line is at 8333 eV, the Ni K adsorption edge. The segregation profile obtained from the SXRD measurements is shown in the center of the figure (reproduced with permission from reference [81]).

Figure 12. Potential-dependent measurements of the $Pt_3Ni(111)$ and Pt(111) crystal surfaces. **(a)** XRV measurements for $Pt_3Ni(111)$ at the (0, 0, 2.7) (red line) and Pt(111) at (1, 0, 3.6) (blue line) with 2 mV/s sweep rate. **(b)** Cyclic voltammetry recorded in 0.1 M $HClO_4$ with 50 mV/s sweep rate. **(c)** Surface coverage by underpotentially deposited hydrogen (H_{upd}) and hydroxyl species (OH_{ad}) calculated from the cyclic voltammograms of $Pt_3Ni(111)$ (red curve) and Pt(111) (blue curve) (reproduced with permission from reference [81]).

Figure 13. A schematic illustration of the interface structure at the negatively charged (left) and positively charged (right) Ag(111) surface in 0.1 M KOH electrolyte. The models were

obtained from the CTR data measured at -1.0 V (circles) and -0.2 V (squares) versus SCE **(a)** the specular CTR, (0, 0, L) and **(b)** a non-specular CTR, (1, 0, L). Data measured at -0.2 V is normalized to the data measured at -1.0 V and shown in **(c)** and **(d)**. The solid lines are fits to the data which yield the structural models (adapted with permission from reference [22]).

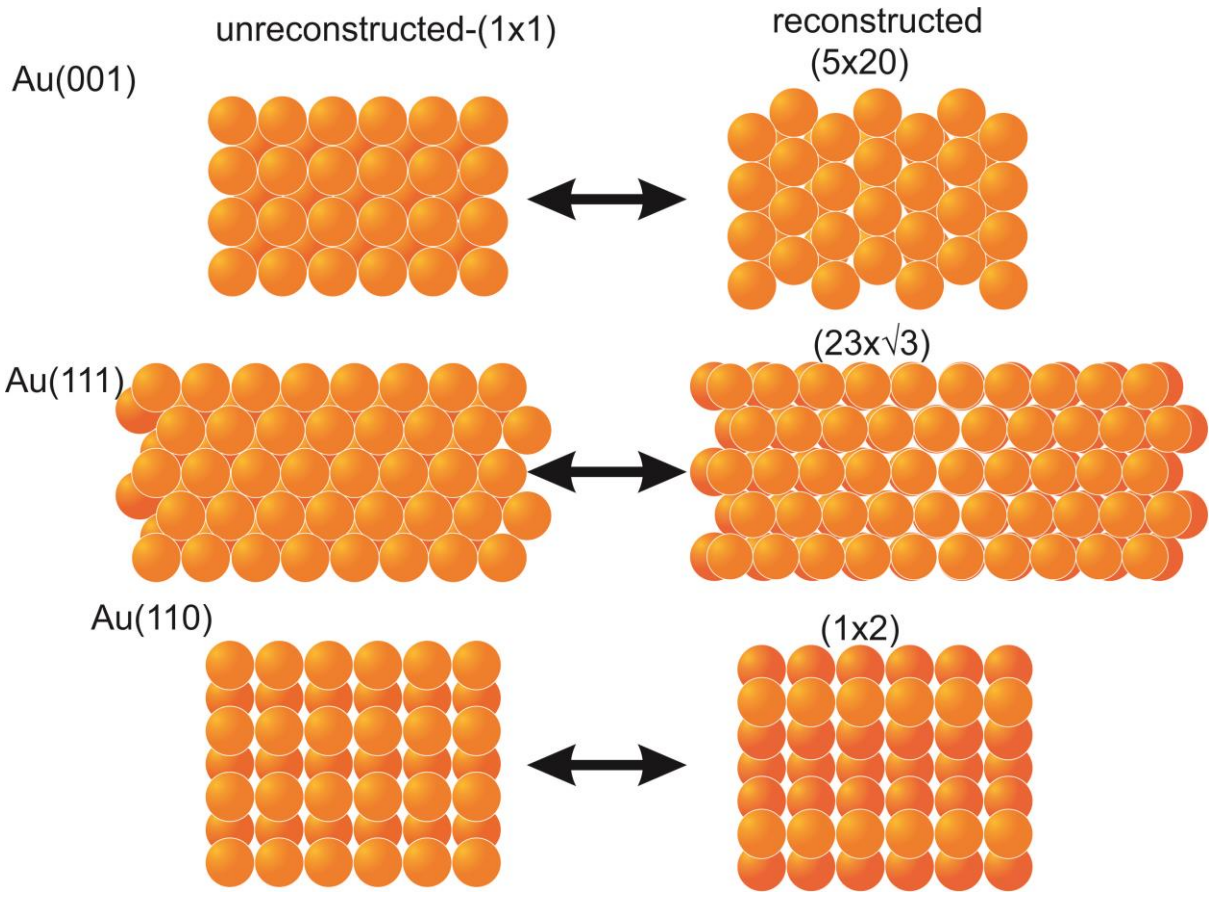
unreconstructed-(1x1)
reconstructed
(5x20)
Au(001)
(23x√3)
Au(111)
Au(110)
(1x2)

Figure 1

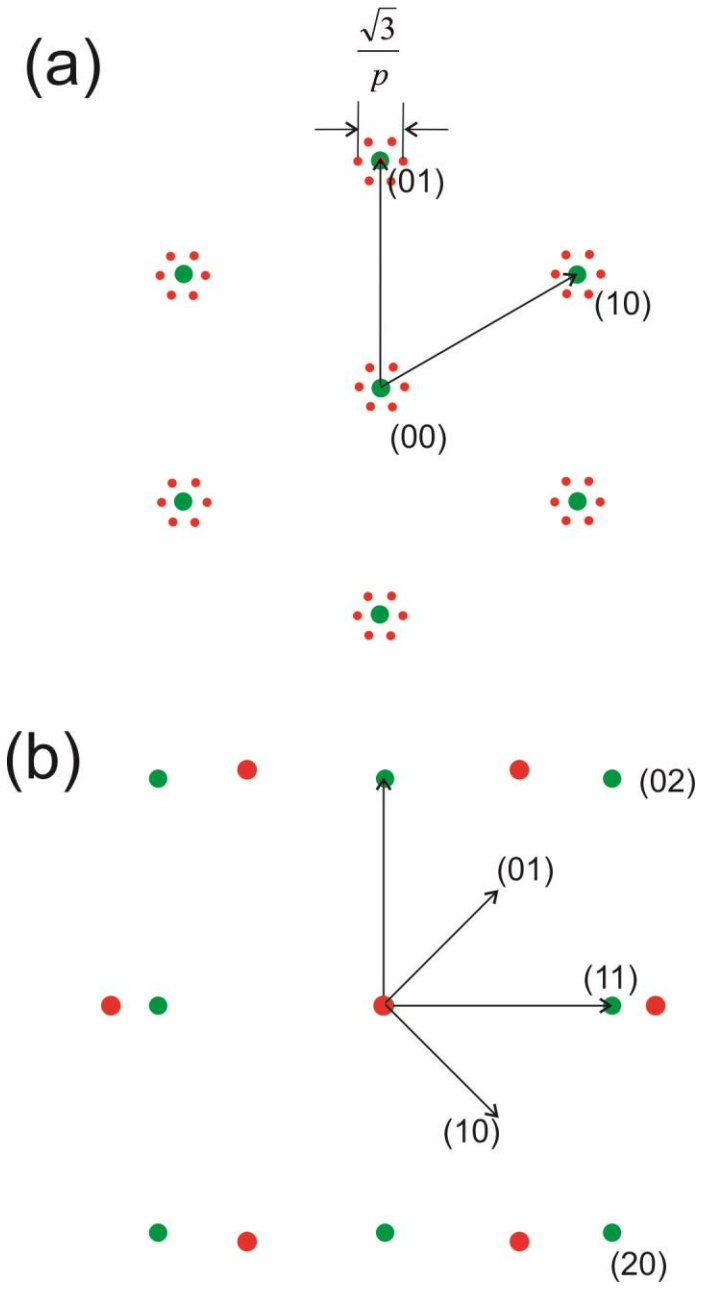

Figure 2

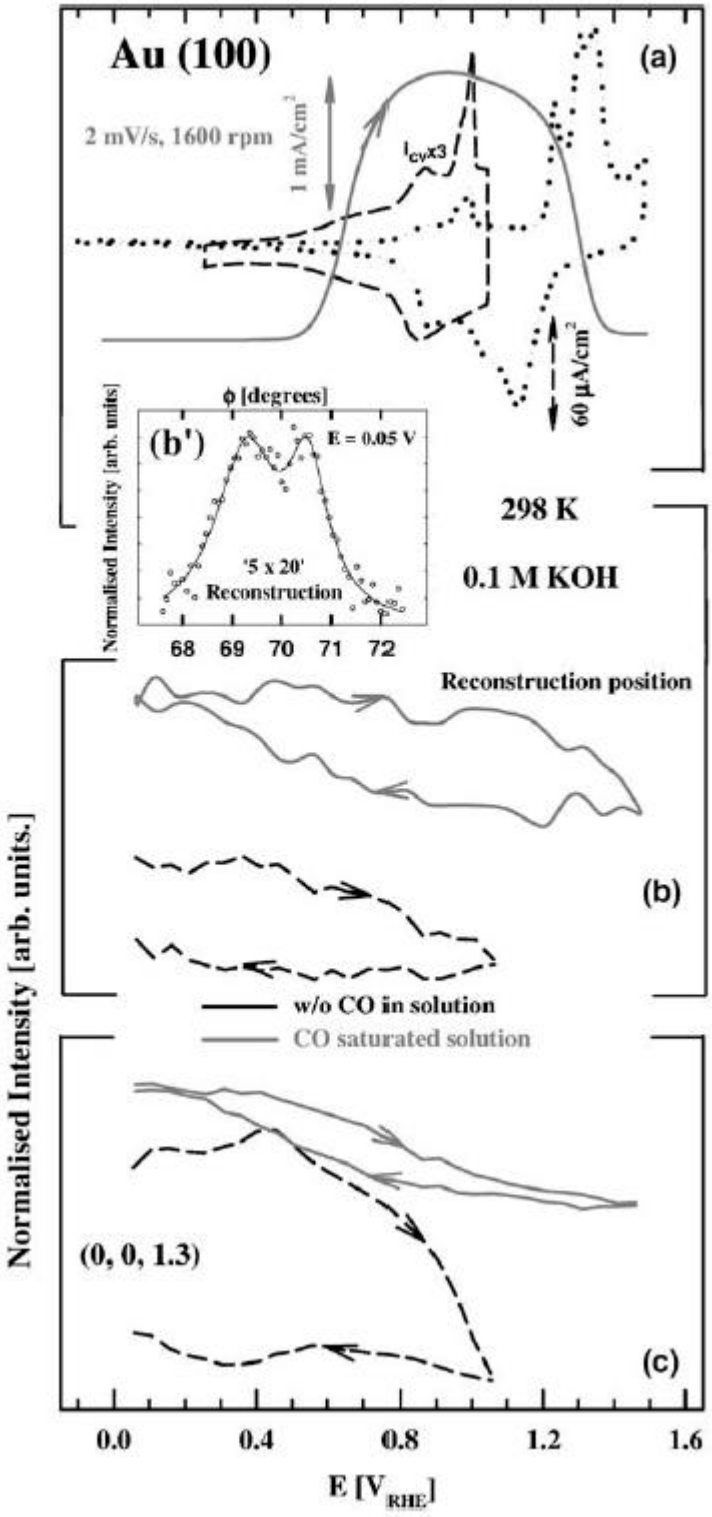
Au (100)
(a)
2 mV/s, 1600 rpm
1 mA/cm²
I_cvx3
60 µA/cm²
ϕ [degrees]
(b')
E = 0.05 V
'5 x 20'
Reconstruction
Normalised Intensity [arb. units]
68 69 70 71 72
298 K
0.1 M KOH
Reconstruction position
(b)
w/o CO in solution
CO saturated solution
(0, 0, 1.3)
(c)
Normalised Intensity [arb. units.]
0.0 0.4 0.8 1.2 1.6
E [V_RHE]

Figure 3

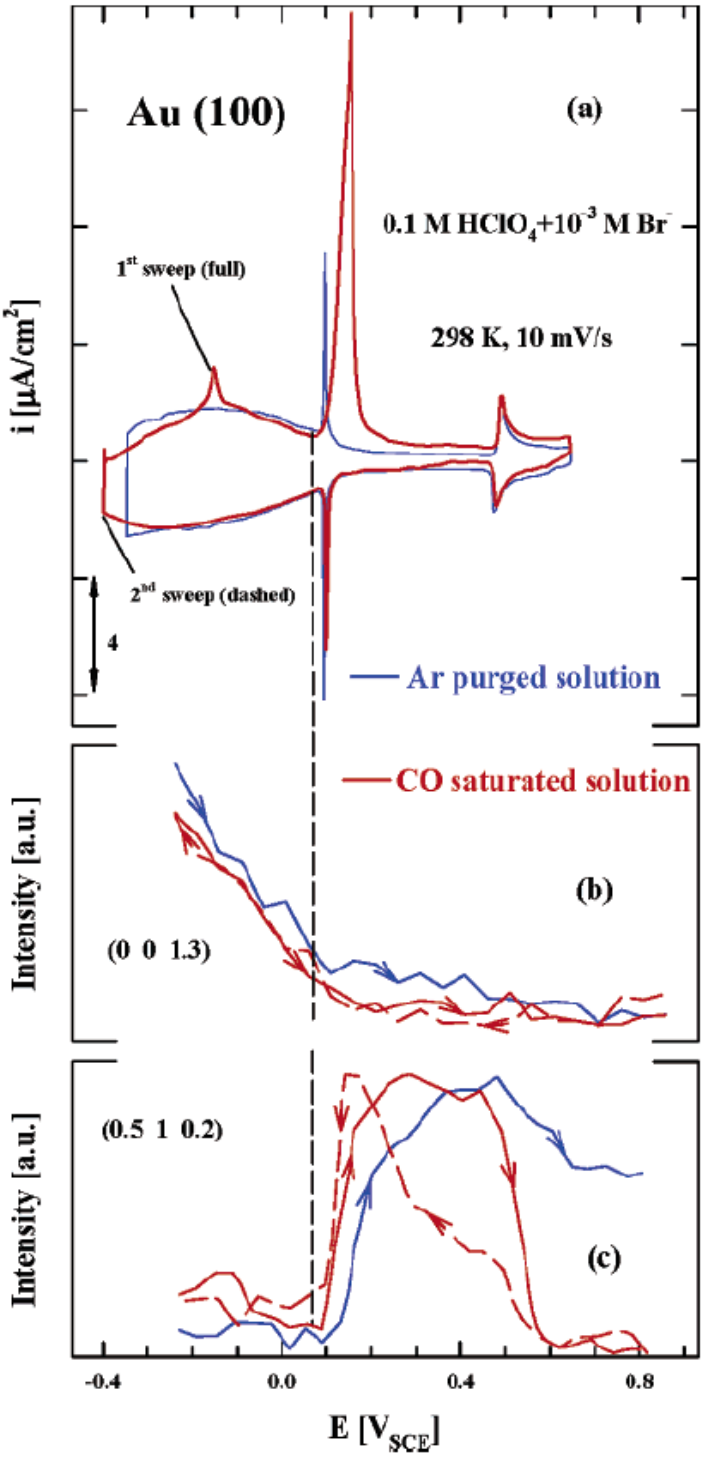
Au (100)
(a)
0.1 M HClO4+10-3 M Br-
1st sweep (full)
298 K, 10 mV/s
2nd sweep (dashed)
4
Ar purged solution
CO saturated solution
i [μA/cm2]
Intensity [a.u.]
(b)
(0 0 1.3)
(0.5 1 0.2)
(c)
-0.4
0.0
0.4
0.8
E [VSCE]

Figure 4

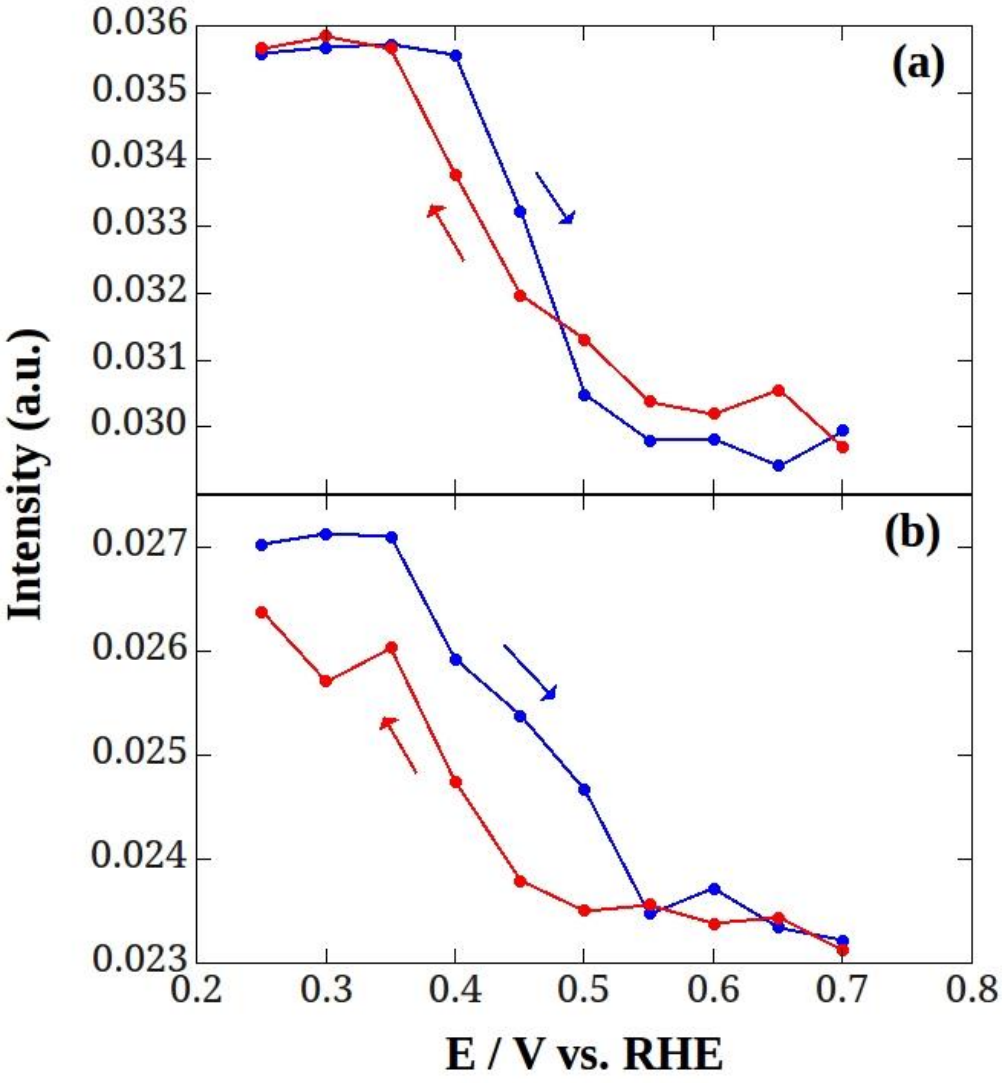
(a)
(b)
Intensity (a.u.)
E / V vs. RHE
0.036
0.035
0.034
0.033
0.032
0.031
0.030
0.027
0.026
0.025
0.024
0.023
0.2
0.3
0.4
0.5
0.6
0.7
0.8

Figure 5

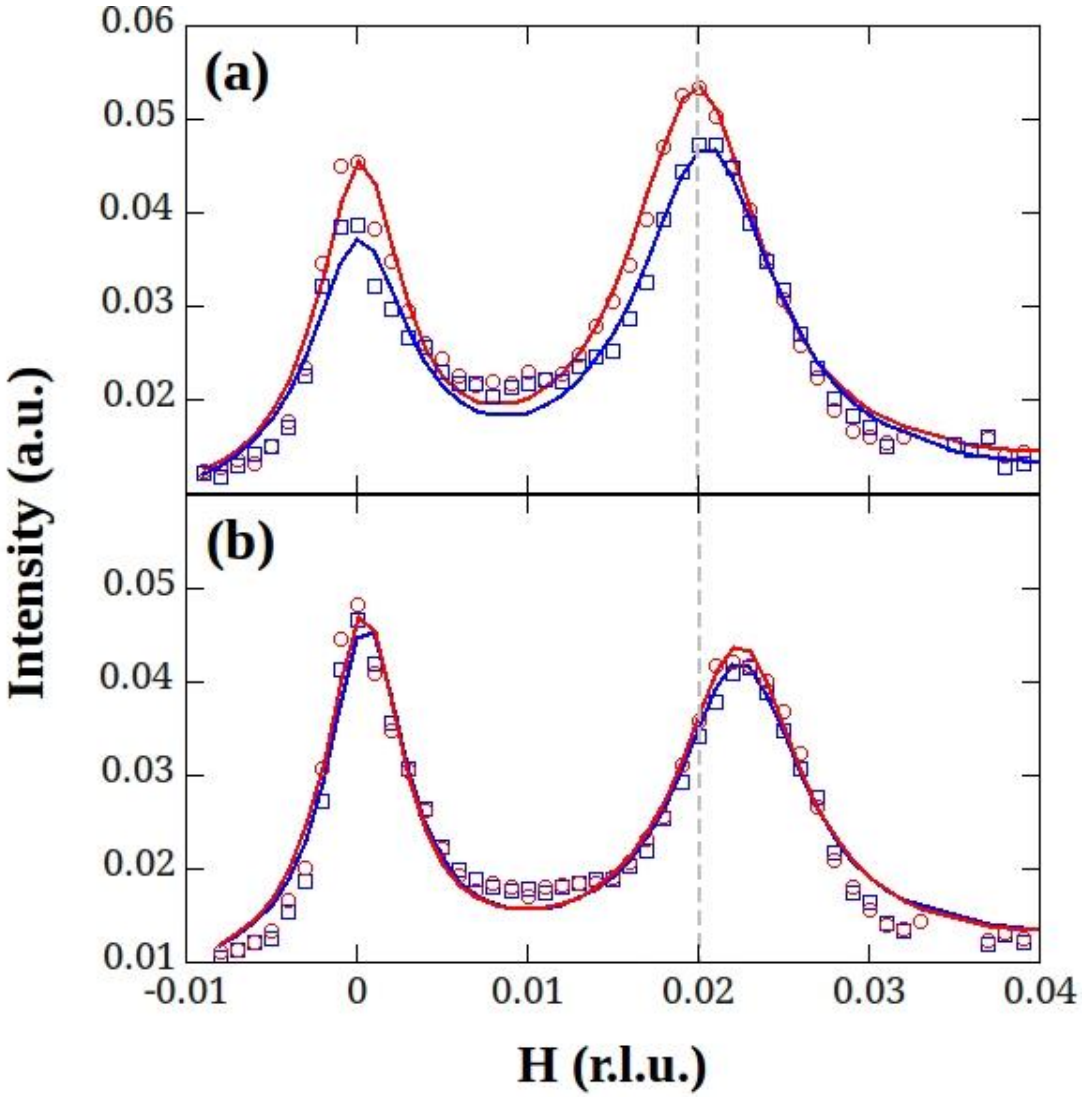
(a)
(b)
Intensity (a.u.)
H (r.l.u.)
0.06
0.05
0.04
0.03
0.02
0.01
-0.01
0
0.01
0.02
0.03
0.04

Figure 6

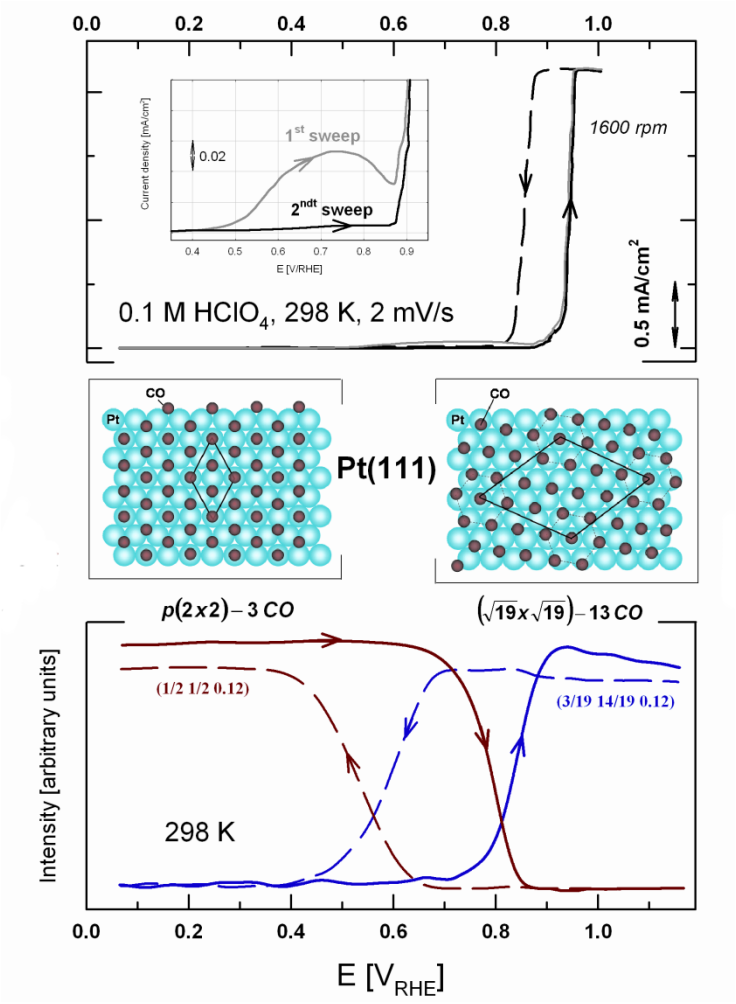
0.0
0.2
0.4
0.6
0.8
1.0
1st sweep
0.02
2ndt sweep
Current density [mA/cm²]
E [V/RHE]
1600 rpm
0.1 M HClO4, 298 K, 2 mV/s
0.5 mA/cm²
CO
Pt
Pt(111)
p(2x2)–3 CO
(√19x√19)–13 CO
(1/2 1/2 0.12)
(3/19 14/19 0.12)
298 K
Intensity [arbitrary units]
E [VRHE]

Figure 7

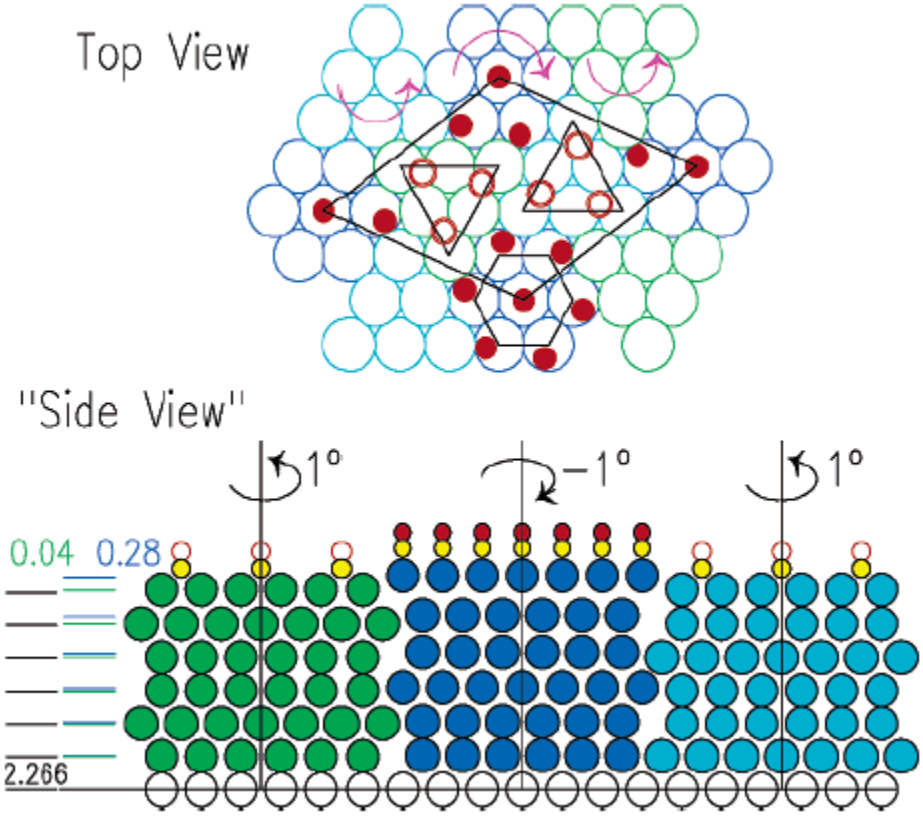

Figure 8

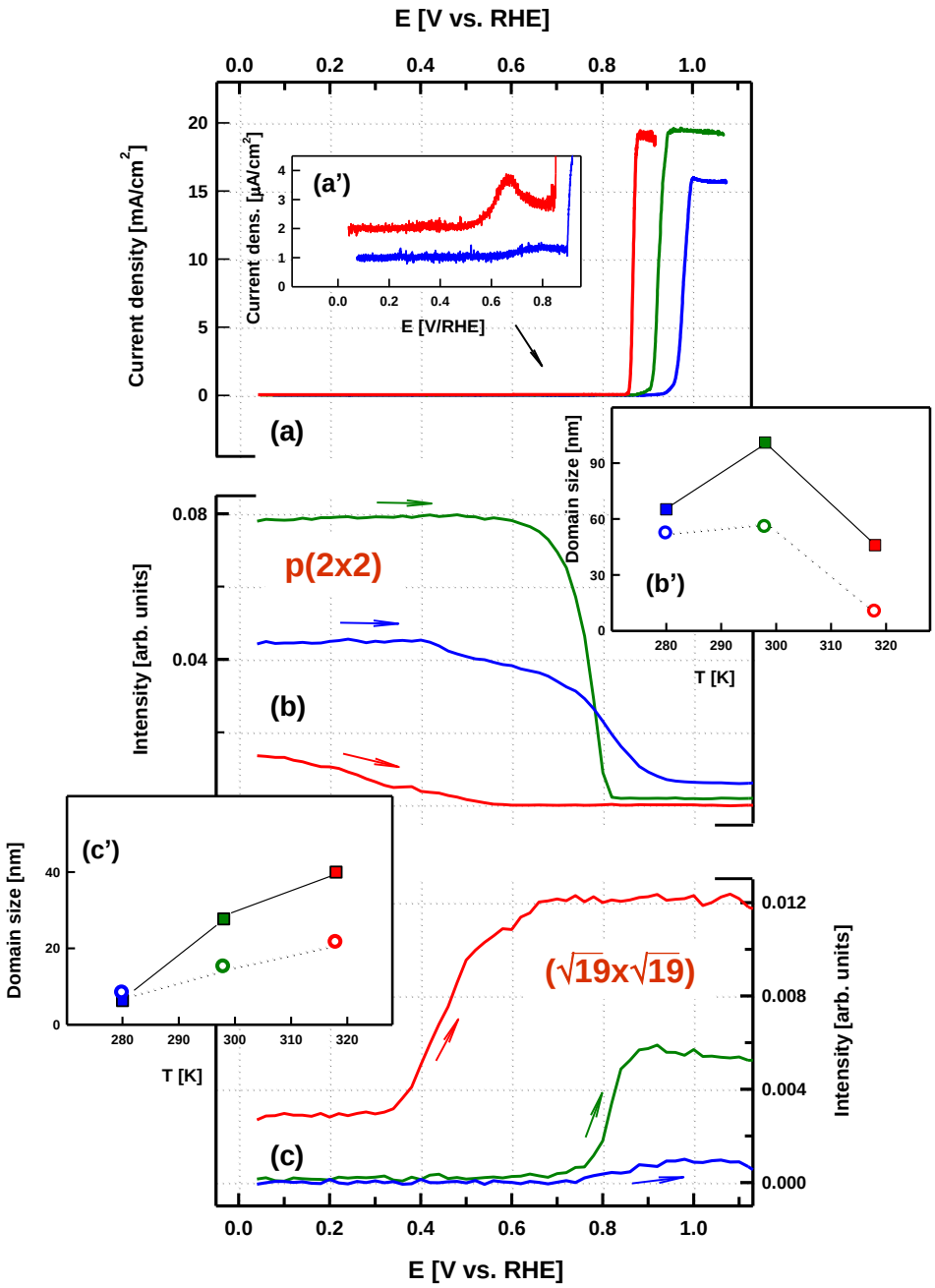
E [V vs. RHE]
Current density [mA/cm^2]
Current dens. [μA/cm^2]
(a')
E [V/RHE]
(a)
Domain size [nm]
(b')
T [K]
Intensity [arb. units]
p(2x2)
(b)
Domain size [nm]
(c')
T [K]
(√19x√19)
(c)
Intensity [arb. units]
E [V vs. RHE]

Figure 9

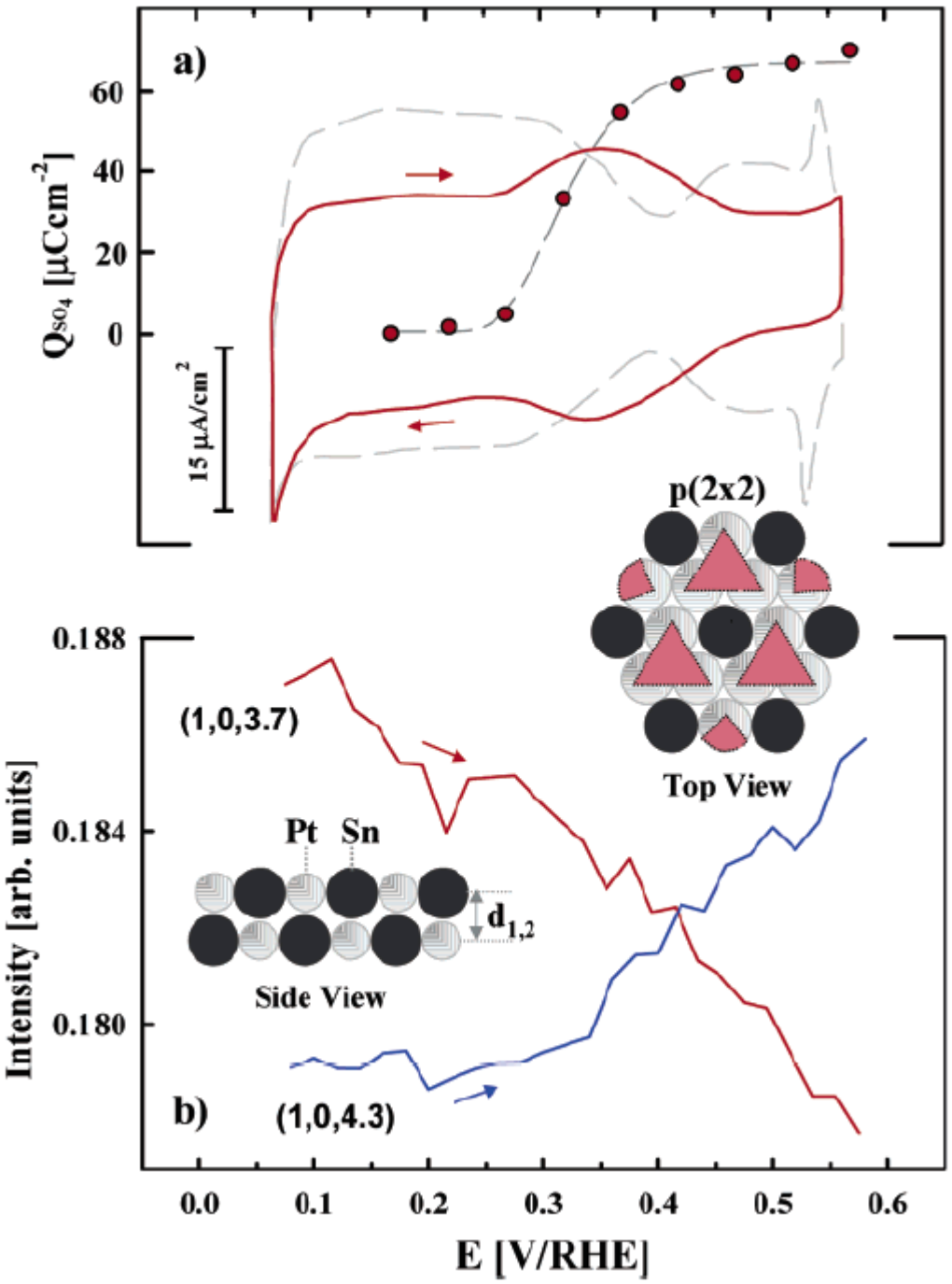
a)
60
40
20
0
Q_{SO_4} [μCcm^{-2}]
15 μA/cm^2
p(2x2)
Top View
0.188
0.184
0.180
Intensity [arb. units]
(1,0,3.7)
Pt Sn
$d_{1,2}$
Side View
b)
(1,0,4.3)
0.0
0.1
0.2
0.3
0.4
0.5
0.6
E [V/RHE]

Figure 10

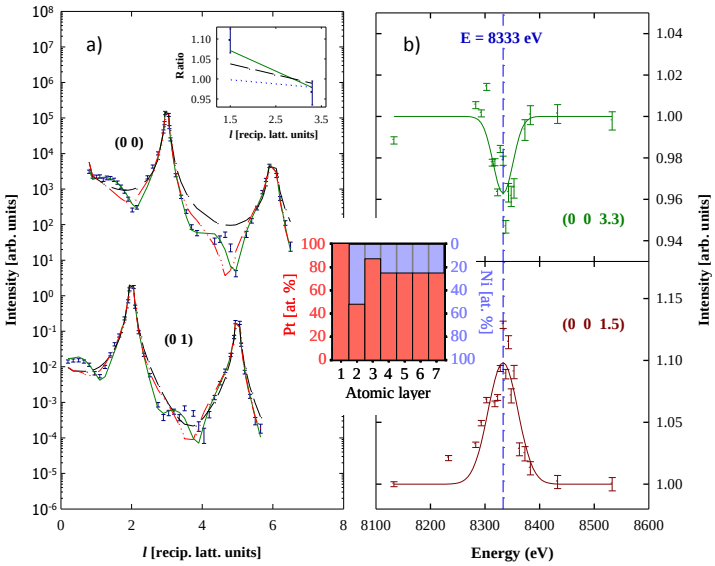
a)
b)
E = 8333 eV
(0 0)
(0 1)
(0 0 3.3)
(0 0 1.5)
Ratio
l [recip. latt. units]
Intensity [arb. units]
Energy (eV)
Pt [at. %]
Ni [at. %]
Atomic layer

Figure 11

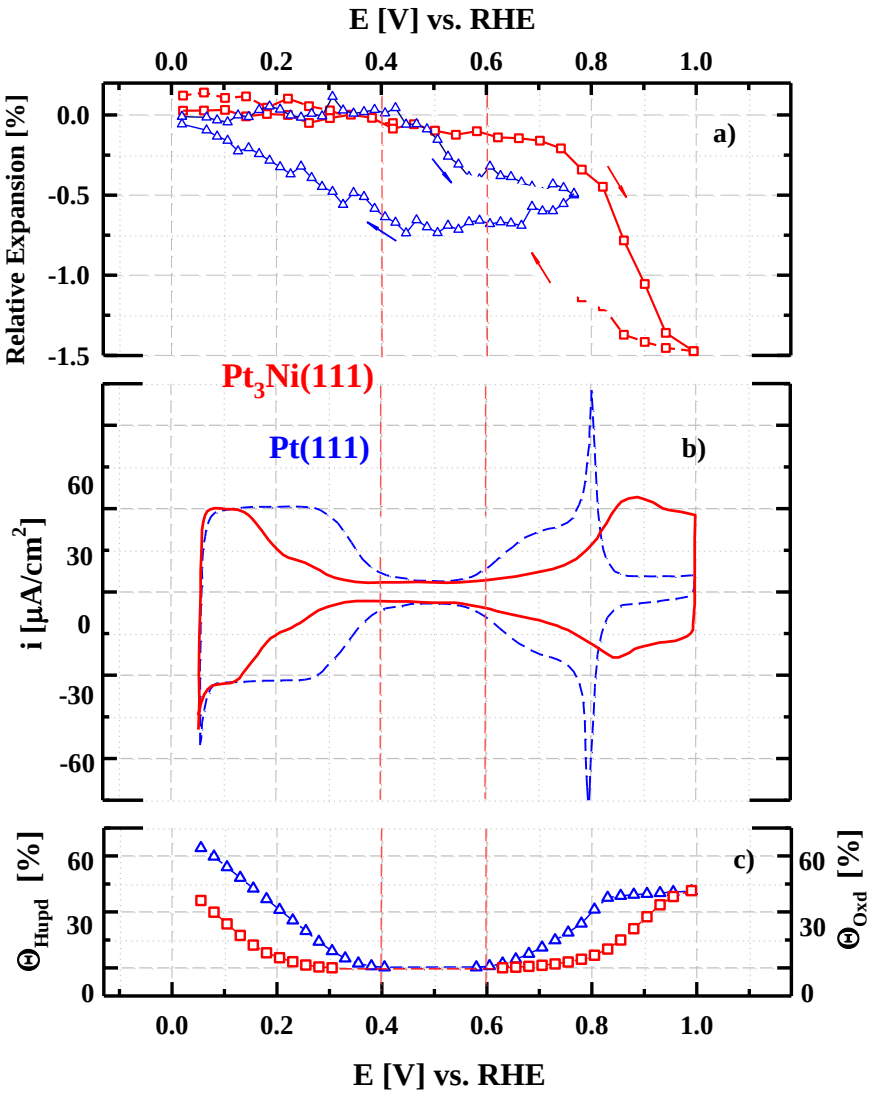
E [V] vs. RHE
0.0
0.2
0.4
0.6
0.8
1.0
Relative Expansion [%]
0.0
-0.5
-1.0
-1.5
a)
Pt3Ni(111)
Pt(111)
b)
i [µA/cm2]
60
30
0
-30
-60
c)
ΘHupd [%]
ΘOxd [%]
60
30
0
E [V] vs. RHE

Figure 12

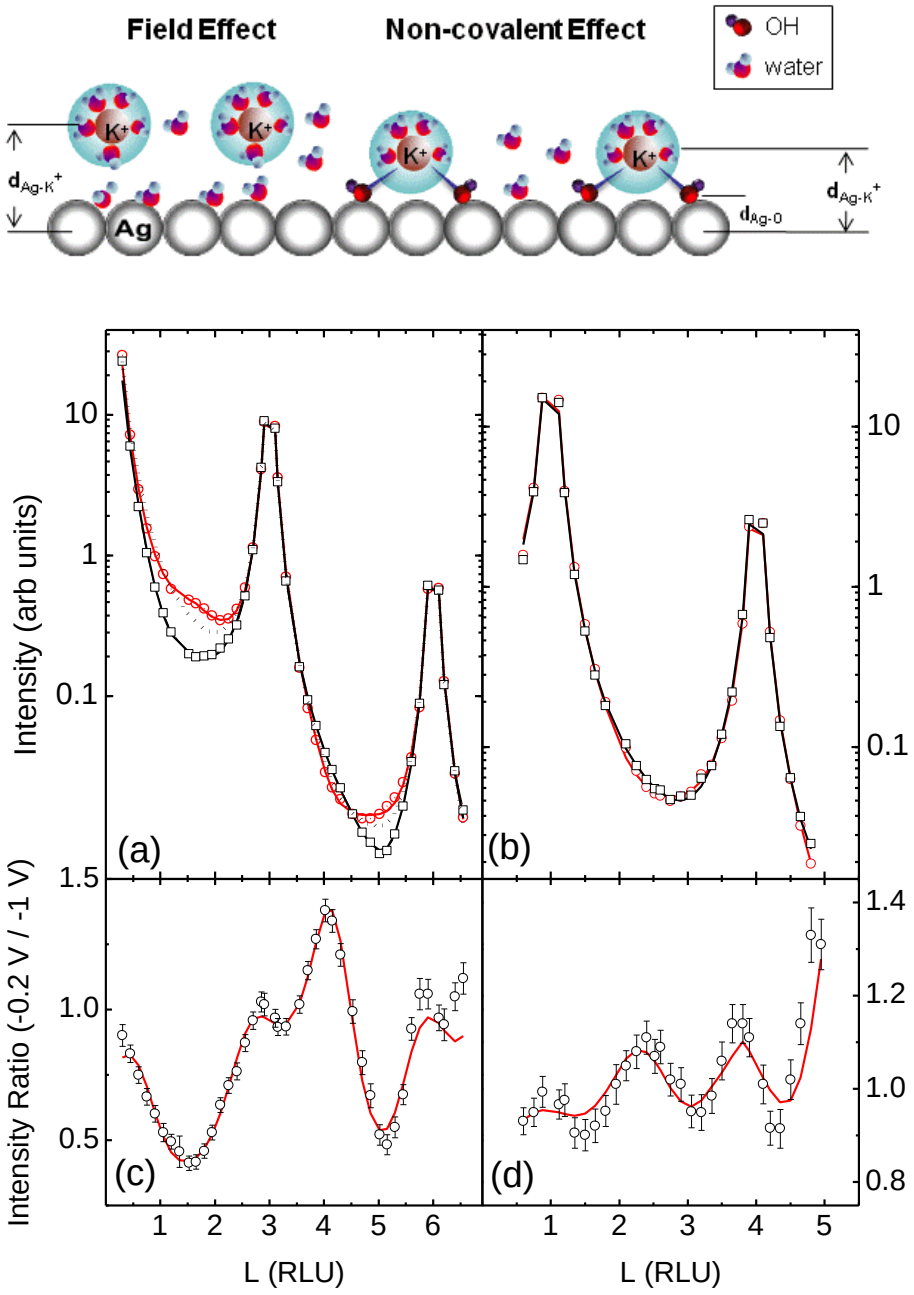
Field Effect
Non-covalent Effect
OH
water
K+
Ag
d Ag-K+
d Ag-O
Intensity (arb units)
Intensity Ratio (-0.2 V / -1 V)
(a)
(b)
(c)
(d)
L (RLU)
L (RLU)

Figure 13

References

[1] M.G. Samant, M.F. Toney, G.L. Borges, L. Blum, O.R. Melroy, Journal of Physical Chemistry, 92 (1988) 220-225.
[2] M.G. Samant, M.F. Toney, G.L. Borges, L. Blum, O.R. Melroy, Surface Science, 193 (1988) L29-L36.
[3] I.M. Tidswell, N.M. Marković, C.A. Lucas, P.N. Ross, Physical Review B, 47 (1993) 16542-16553.
[4] I.M. Tidswell, N.M. Marković, P.N. Ross, Physical Review Letters, 71 (1993) 1601-1604.
[5] B.M. Ocko, O.M. Magnussen, R.R. Adžić, J.X. Wang, Z. Shi, J. Lipkowski, Journal of Electroanalytical Chemistry, 376 (1994) 35-39.
[6] I.M. Tidswell, N.M. Markovic, P.N. Ross, Journal of Electroanalytical Chemistry, 376 (1994) 119-126.
[7] I.M. Tidswell, N.M. Marković, P.N. Ross, Surface Science, 317 (1994) 241-252.
[8] C.A. Lucas, N.M. Marković, P.N. Ross, Surface Science, 340 (1995) L949-L954.
[9] N.M. Marković, H.A. Gasteiger, C.A. Lucas, I.M. Tidswell, P.N. Ross Jr, Surface Science, 335 (1995) 91-100.
[10] I.M. Tidswell, C.A. Lucas, N.M. Marković, P.N. Ross, Physical Review B, 51 (1995) 10205-10208.
[11] E. Herrero, L.J. Buller, H.D. Abruña, Chemical Reviews, 101 (2001) 1897-1930.
[12] O.M. Magnussen, Chemical Reviews, 102 (2002) 679-725.
[13] C.A. Lucas, N.M. Markovic, In-situ Surface X-ray Scattering and Infrared Reflection Adsorption Spectroscopy of CO Chemisorption at the Electrochemical Interface, In-situ Spectroscopic Studies of Adsorption at the Electrode and Electrocatalysis, 2007, pp. 339-381.
[14] C.A. Lucas, N.M. Markovic, in: R.C. Alkire, D.M. Kolb, J. Lipkowski, P.N. Ross (Eds.) Advances in Electrochemical Science and Engineering, 2006.
[15] M. Mercer, H. Hoster, Nano Energy.
[16] S. Cherevko, N. Kulyk, K.J.J. Mayrhofer, Nano Energy.
[17] H. Lv, D. Li, D. Strmcnik, A.P. Paulikas, N.M. Markovic, V.R. Stamenkovic, Nano Energy.
[18] R. Feidenhans'l, Surf.Sc.Reports, 10 (1989) 105-188.
[19] P.H. Fuoss, S. Brennan, Annual Review of Materials Science, 20 (1990) 365-390.
[20] I.K. Robinson, D.J. Tweet, Reports on Progress in Physics, 55 (1992) 599-651.

[21] I.K. Robinson, Physical Review B, 33 (1986) 3830-3836.
[22] C.A. Lucas, P. Thompson, Y. Gründer, N.M. Markovic, Electrochemistry Communications, 13 (2011) 1205-1208.
[23] P. Fenter, N.C. Sturchio, Progress in Surface Science, 77 (2005) 171-258.
[24] C.A. Lucas, N.M. Markovic, Structure Relationships in Electrochemical Reactions, in: A.J. Bard, M. Stratmann, E.J. Calvo (Eds.) Encyclopedia of Electrochemistry: Interfacial Kinetics and Mass Transport, Wiley VCH, Weinheim, 2004, pp. 295-360.
[25] C.A. Lucas, N.M. Marković, P.N. Ross, Surface Science, 448 (2000) 77-86.
[26] C.A. Lucas, N.M. Marković, B.N. Grgur, P.N. Ross, Surface Science, 448 (2000) 65-76.
[27] J. Clavilier, J.Electroanal.Chem., 107 (1980) 211-216.
[28] N. Markovic, M. Hanson, G. McDougall, E. Yeager, Journal of Electroanalytical Chemistry, 214 (1986) 555-566.
[29] R.F. Saraf, C. Dimitrakopoulos, M.F. Toney, S.P. Kowalczyk, Langmuir, 12 (1996) 2802-2806.
[30] Y.S. Chu, University of Illinois at Urbana-Champaign1997.
[31] O.M. Magnussen, J. Scherer, B.M. Ocko, R.J. Behm, J.Phys.Chem.B, 104 (2000) 1222-1226.
[32] J. Wang, A.J. Davenport, H.S. Isaacs, B.M. Ocko, Science, 255 (1992) 1416-1418.
[33] B.M. Ocko, J. Wang, A. Davenport, H. Isaacs, Physical Review Letters, 65 (1990) 1466-1469.
[34] B.M. Ocko, G. Helgesen, B.C. Schardt, J. Wang, Phys.Rev.Lett., 69 (1992) 3350-3353.
[35] B.B. Blizanac, C.A. Lucas, M.E. Gallagher, P.N. Ross, N.M. Marković, Journal of Physical Chemistry B, 108 (2004) 5304-5313.
[36] D.M. Kolb, Progress in Surface Science, 51 (1996) 109-173.
[37] K.P. Bohnen, D.M. Kolb, Surf.Sci., 407 (1998) L629-L632.
[38] G.J. Edens, X. Gao, M.J. Weaver, N.M. Markovic, P.N. Ross, Surface Science, 302 (1994) L275-L282.
[39] M.E. Gallagher, B.B. Blizanac, C.A. Lucas, P.N. Ross, N.M. Marković, Surface Science, 582 (2005) 215-226.
[40] B.B. Blizanac, C.A. Lucas, M.E. Gallagher, M. Arenz, P.N. Ross, N.M. Marković, Journal of Physical Chemistry B, 108 (2004) 625-634.
[41] J.X. Wang, N.S. Marinkovic, R.R. Adzic, Colloid and Surfaces A, 134 (1998) 165-171.
[42] R.R. Adžić, J.X. Wang, Electrochimica Acta, 45 (2000) 4203-4210.

[43] P. Rodriguez, J.M. Feliu, M.T.M. Koper, Electrochemistry Communications, 11 (2009) 1105-1108.
[44] P. Rodriguez, Y. Kwon, M.T.M. Koper, Nature Chemistry, 4 (2012) 177-182.
[45] P. Rodriguez, N. Garcia-Araez, M.T.M. Koper, Physical Chemistry Chemical Physics, 12 (2010) 9373-9380.
[46] P. Rodriguez, N. Garcia-Araez, A. Koverga, S. Frank, M.T.M. Koper, Langmuir, 26 (2010) 12425-12432.
[47] P. Rodríguez, A.A. Koverga, M.T.M. Koper, Angewandte Chemie - International Edition, 49 (2010) 1241-1243.
[48] D.M. Kolb, J. Schneider, Electrochim.Acta, 31 (1986) 929-936.
[49] A.R. Sandy, S.G.J. Mochrie, D.M. Zehner, G. Grübel, K.G. Huang, D. Gibbs, Phys.Rev.Lett., 68 (1992) 2192-2195.
[50] G. Harlow, Y. Grunder, N. Sisson, P. Thompson, E. Cocklin, C.A. Lucas.
[51] B.L.M. Hendriksen, S.C. Bobaru, J.W.M. Frenken, Topics in Catalysis, 36 (2005) 43-54.
[52] M.D. Ackermann, T.M. Pedersen, B.L.M. Hendriksen, O. Robach, S.C. Bobaru, I. Popa, C. Quiros, H. Kim, B. Hammer, S. Ferrer, J.W.M. Frenken, Physical Review Letters, 95 (2005).
[53] N.M. Markovíc, P.N. Ross Jr, Surface Science Reports, 45 (2002) 117-229.
[54] N.M. Marković, P.N. Ross, Electrochimica Acta, 45 (2000) 4101-4115.
[55] K.J.J. Mayrhofer, M. Arenz, B.B. Blizanac, V. Stamenkovic, P.N. Ross, N.M. Markovic, Electrochimica Acta, 50 (2005) 5144-5154.
[56] N.M. Marković, B.N. Grgur, C.A. Lucas, P.N. Ross, Surface Science, 384 (1997) L805-L814.
[57] C.A. Lucas, N.M. Marković, P.N. Ross, Physical Review Letters, 77 (1996) 4922-4925.
[58] N.M. Marković, C.A. Lucas, B.N. Grgur, P.N. Ross, Journal of Physical Chemistry B, 103 (1999) 9616-9623.
[59] N.M. Marković, C.A. Lucas, A. Rodes, V. Stamenkovíc, P.N. Ross, Surface Science, 499 (2002) L149-L158.
[60] I. Villegas, M.J. Weaver, The Journal of Chemical Physics, 101 (1994) 1648-1660.
[61] I. Villegas, X. Gao, M.J. Weaver, Electrochimica Acta, 40 (1995) 1267-1275.
[62] C.A. Lucas, N.M. Marković, P.N. Ross, Surface Science, 425 (1999) L381-L386.
[63] N.M. Marković, B.N. Grgur, C.A. Lucas, P.N. Ross, Journal of Physical Chemistry B, 103 (1999) 487-495.

[64] Y.V. Tolmachev, A. Menzel, A.V. Tkachuk, Y.S. Chu, H. You, Electrochemical and Solid-State Letters, 7 (2004) E23-E26.
[65] D.S. Strmcnik, P. Rebec, M. Gaberscek, D. Tripkovic, V. Stamenkovic, C. Lucas, N.M. Markovic, Journal of Physical Chemistry C, 111 (2007) 18672-18678.
[66] J.X. Wang, I.K. Robinson, B.M. Ocko, R.R. Adzic, Journal of Physical Chemistry B, 109 (2005) 24-26.
[67] C.A. Lucas, P. Thompson, M. Cormack, A. Brownrigg, B. Fowler, D. Strmcnik, V. Stamenkovic, J. Greeley, A. Menzel, H. You, N.M. Markovic, Journal of the American Chemical Society, 131 (2009) 7654-7661.
[68] J.-Y. Ye, Y.-X. Jiang, T. Sheng, S.G. Sun, Nano Energy, this issue (2016).
[69] N.M. Marković, B.N. Grgur, C.A. Lucas, P.N. Ross, Langmuir, 16 (2000) 1998-2005.
[70] J.A. Rodriguez, Surface Science Reports, 24 (1996) 223-287.
[71] V.R. Stamenkovic, N.M. Markovic, Catalysis at bimetallic electrochemical interfaces, Model Systems in Catalysis: Single Crystals to Supported Enzyme Mimics, 2010, pp. 51-73.
[72] V. Stamenković, M. Arenz, B.B. Blizanac, K.J.J. Mayrhofer, P.N. Ross, N.M. Marković, Surface Science, 576 (2005) 145-157.
[73] V.R. Stamenkovic, B. Fowler, B.S. Mun, G. Wang, P.N. Ross, C.A. Lucas, N.M. Markovic, Science, 315 (2007) 493-497.
[74] M.E. Gallagher, C.A. Lucas, V. Stamenković, N.M. Marković, P.N. Ross, Surface Science, 544 (2003) L729-L734.
[75] V.R. Stamenković, M. Arenz, C.A. Lucas, M.E. Gallagher, P.N. Ross, N.M. Marković, Journal of the American Chemical Society, 125 (2003) 2736-2745.
[76] T.E. Shubina, M.T.M. Koper, Electrochimica Acta, 47 (2002) 3621-3628.
[77] V.R. Stamenkovic, B.S. Mun, M. Arenz, K.J.J. Mayrhofer, C.A. Lucas, G. Wang, P.N. Ross, N.M. Markovic, Nature Materials, 6 (2007) 241-247.
[78] T. Toda, H. Igarashi, M. Watanabe, Journal of the Electrochemical Society, 145 (1998) 4185-4188.
[79] T. Toda, H. Igarashi, M. Watanabe, Journal of Electroanalytical Chemistry, 460 (1999) 258-262.
[80] T. Toda, H. Igarashi, H. Uchida, M. Watanabe, Journal of the Electrochemical Society, 146 (1999) 3750-3756.
[81] B. Fowler, C.A. Lucas, A. Omer, G. Wang, V.R. Stamenković, N.M. Marković, Electrochimica Acta, 53 (2008) 6076-6080.
[82] B.E. Warren, X-ray diffraction, Dover Publications Inc., 1990.

[83] V. Stamenkovic, B.S. Mun, K.J.J. Mayrhofer, P.N. Ross, N.M. Markovic, J. Rossmeisl, J. Greeley, J.K. Nørskov, Angewandte Chemie - International Edition, 45 (2006) 2897-2901.
[84] H. You, Z. Nagy, Physica B: Physics of Condensed Matter, 198 (1994) 187-194.
[85] M. Labayen, C. Ramirez, W. Schattke, O.M. Magnussen, Nature Materials, 2 (2003) 783-787.
[86] F.U. Renner, Y. Gründer, J. Zegenhagen, Rev.Sci.Instrum., 78 (2007) 033903.
[87] C.A. Lucas, M. Cormack, M.E. Gallagher, A. Brownrigg, P. Thompson, B. Fowler, Y. Gründer, J. Roy, V. Stamenković, N.M. Marković, Faraday Discussions, 140 (2008) 41-58.
[88] F. McBride, G.R. Darling, K. Pussi, C.A. Lucas, Y. Gründer, M. Darlington, A. Brownrigg, A. Hodgson, Journal of Physical Chemistry C, 117 (2013) 4032-4039.
[89] F.U. Renner, A. Stierle, H. Dosch, D.M. Kolb, T.L. Lee, J. Zegenhagen, Nature, 439 (2006) 707-710.
[90] J. Suntivich, K.J. May, H.A. Gasteiger, J.B. Goodenough, Y. Shao-Horn, Science, 334 (2011) 1383-1385.
[91] J. Herranz, J. Durst, E. Fabbri, A. Patru, X. Cheng, A.A. Permyakova, T.J. Schmidt, Nano Energy.
[92] S.J. Tauster, Accounts of Chemical Research, 20 (1987) 389-394.
[93] M.F. Toney, J.N. Howard, J. Richer, G.L. Borges, J.G. Gordon, O.R. Melroy, D.G. Wiesler, D. Yee, L.B. Sorensen, Nature, 368 (1994) 444-446.
[94] M.F. Toney, J.N. Howard, J. Richer, G.L. Borges, J.G. Gordon, O.R. Melroy, D.G. Wiesler, D. Yee, L.B. Sorensen, Surface Science, 335 (1995) 326-332.
[95] D. Strmcnik, K. Kodama, D. Van Der Vliet, J. Greeley, V.R. Stamenkovic, N.M. Marković, Nature Chemistry, 1 (2009) 466-472.
[96] M. Nakamura, Y. Nakajima, N. Hoshi, H. Tajiri, O. Sakata, ChemPhysChem, 14 (2013) 2426-2431.
[97] D. Strmcnik, D.F. Van Der Vliet, K.C. Chang, V. Komanicky, K. Kodama, H. You, V.R. Stamenkovic, N.M. Marković, Journal of Physical Chemistry Letters, 2 (2011) 2733-2736.
[98] Z. Zeng, J. Greeley, Nano Energy, this issue (2016).
[99] M. Mezger, H. Schröder, H. Reichert, S. Schramm, J.S. Okasinski, S. Schöder, V. Honkimäki, M. Deutsch, B.M. Ocko, J. Ralston, M. Rohwerder, M. Stratmann, H. Dosch, Science, 322 (2008) 424-428.
[100] F. Golks, Y. Gründer, J. Stettner, K. Krug, J. Zegenhagen, O.M. Magnussen, Surface Science, 631 (2014) 112-122.

[101] F. Golks, K. Krug, Y. Gründer, J. Zegenhagen, J. Stettner, O.M. Magnussen, Journal of the American Chemical Society, 133 (2011) 3772-3775.
[102] F. Golks, J. Stettner, Y. Gründer, K. Krug, J. Zegenhagen, O.M. Magnussen, Phys. Rev. Lett., 108 (2011) 256101.
[103] K. Krug, D. Kaminski, F. Golks, J. Stettner, O.M. Magnussen, Journal of Physical Chemistry C, 114 (2010) 18634-18644.

Yvonne Gründer's research interests are focussed on atomic scale understanding of the structure and reactions at electrochemical interfaces. During her PhD, which was carried out at the European Synchrotron Radiation Source in Grenoble (France), she studied copper electrodeposition onto GaAs surfaces by in–situ X-ray Diffraction. She then took up postdoctoral positions, at the Christian-Albrechts-Universität in Kiel (Germany), where she studied homoepitaxial electrodeposition by in-situ x-ray scattering and electrochemical techniques and at the University of Manchester, UK, where she investigated nucleation and electrodeposition at liquid-liquid interfaces. She joined the Department of Physics and the Stephenson Institute for Renewable Energy at the University of Liverpool as a Royal Society University Research Fellow in 2012.

Christopher Lucas is a Professor of Physics and Head of the Condensed Matter Physics group at the University of Liverpool. His research focuses on the application of synchrotron radiation techniques to probe structure and reactivity at surfaces and interfaces. He has published over 80 refereed articles in scientific journals and several invited book chapters. He completed his PhD at the University of Edinburgh in 1989, worked at the Lawrence Berkeley National Laboratory from 1990-97 and moved to the Liverpool in 1997. He is the Director of the UK CRG beamline (XMaS) at the European Synchrotron Radiation Facility (ESRF) and has been project spokesperson on experiments at the ESRF, Diamond Light Source (UK), the NSLS, SSRL and APS in the US and the Swiss Light Source.